NTNU

Norwegian University of
Science and Technology

Predicting Porosity and Clay Trends from P-Wave Velocity

Anne Cathrine Helle

Petroleum Geoscience and Engineering
Submission date: June 2018
Supervisor: Kenneth Duffaut, IGP

Norwegian University of Science and Technology
Department of Geoscience and Petroleum

Preface

This is a Master's thesis in geophysics at NTNU as part of the study program Petroleum Geoscience and Engineering. The project was carried out during the spring semester of 2018.

Trondheim, 2018-06-18

Anne Cathrine Helle

Acknowledgment

I would like to extend my gratitude to my supervisor, Kenneth Duffaut, for his guidance, patience, and commitment to this project, and for making me interested in rock physics through the course Reservoir Seismics. His guidance has been motivating and educating.

A.C.H.

Summary

P-waves are sensitive for several parameters, and when P-waves are the only information present, the primary effects have to be identified. In this study, two models are created to describe the relation between porosity, clay content, and P-wave velocity. The models are constructed by taking base in a sand-clay mixture undergoing mechanical compaction, where the transition from the grain-supported regime to the matrix-supported regime is described. The aim of the study is to investigate if it is possible to predict porosity and clay content solely based on P-wave velocities.

The two models are based on Dvorkin's Textural Sorting and the Bound Averaging Method. The Dvorkin model uses the difference in grain sizes to create a porosity model, and the elastic moduli are calculated by using Hertz-Mindlin and Hashin-Shtrikman. The modified Bound Averaging Method model takes base in the Voigt and Reuss bounds, and an anisotropic elastic constant is introduced. In this model, an iso-stress analogue for the Reuss, w, is used to account for changes in stress. The models are compared to lab data and are used to perform porosity and clay content estimations in three wells from the Norwegian Continental Shelf. The sand-clay mixture is assumed to be fully water-saturated and is modeled for different net stresses. The porosity and clay content estimations are carried out by assuming both a hydrostatic case and an overpressured case in the wells.

Both models underpredict the porosity in the transition between the grain-supported regime to the matrix-supported regime when tested on lab data. The velocities are also overpredicted in the transition between the two constituents, where the Dvorkin model yields a stiffer result than the modified Bound Averaging Method model, overestimating the velocities to be $7.5 - 24.2$ % higher relative to the lab data.

When using sonic velocities to predict porosity and clay trends in the wells, the findings show that both models are able to capture the general porosity and clay trends. The models are, however, shown to have difficulty to accurately predict porosity and clay trends in the transition between the grain-supported regime and the matrix-supported regime, where the general trend is an underprediction of porosity, and both an under- and overprediction of clay content. The modified Bound Averaging Method yields better results when more information is available to estimate w, while the Dvorkin model yields better results when information in scarce. The models offer a simple way to conceptualize and explain the complex relation between porosity, clay content, and P-wave velocity.

Sammendrag

P-bølger er sensitive for flere parametere, og når P-bølger er den eneste informasjonen man har tilgjengelig, er det viktig å identifisere de primære effektene. I denne oppgaven har to modeller blitt utviklet for å beskrive forholdet mellom porøsitet, leirinnhold og P-bølgehastighet. Modellene er konstruert ved å ta utgangspunkt i en blanding av sand og leire som er utsatt for mekanisk kompaksjon, hvor overgangen mellom kornbåret og matriksbåret regime er beskrevet. Formålet er å undersøke om det er mulig å predikere porøsitet og leirinnhold kun ved bruk av P-bølgehastigheter.

Dvorkin-modellen benytter seg av forholdet mellom kornstørrelser for å utvikle en modell for porøsitet, hvor de elastiske moduli blir kalkulert ved bruk av Hertz-mindlin og Hashin-Shtrikman. Den modifiserte Bound Averaging Method-modellen tar utgangspunkt i Voigt- og Reuss-grensene og introduserer en anisotrop elastisk konstant. I sistnevnte modell introduseres det en iso-trykk analog for Reuss, w, for å ta hensyn til endringer i trykk. Modellene er sammenlignet med lab-data og er brukt for å estimere porøsitet og leirinnhold på tre brønner fra den norske kontinentalsokkelen. Blandingen av sand og leire er antatt å være 100 % vannmettet og er modellert for ulike trykk. Estimering av porøsitet og leire er blitt gjort for både et hydrotstatisk tilfelle og et tilfelle hvor det blir antatt overtrykk.

Begge modellene underpredikerer porøsiteten i overgangen mellom det kornbåret og matriksbåret regimet når de blir tested på lab-data. Her er også hastighetene overpredikert, hvor Dvorkin-modellen gir et stivere resultat enn den modifiserte versjonen av Bound Averaging Method, og overestimerer hastighetene til å være 7.5 - 24.2 % høyere enn labdataene.

Når modellene blir brukt for å predikere porøsitet og leirinnhold i brønnene, viser begge modellene at de fanger opp de generelle trendene i brønnen. Modellene viser derimot at de har problemer med å gi nøyaktige prediksjoner i overgangen mellom kornbåret og matriksbåret regime, hvor den generelle trenden er en underprediksjon av porøsitet, og både en under- og overprediksjon av leirinnhold. Den modifiserte versjonen av Bound Averaging Method gir et bedre resultat når man har mer informasjon tilgjengelig for å estimere w, mens Dvorkin-modellen gir et bedre resultat når tilgjengelig informasjon er mangelfull. Modellene konseptualiserer og beskriver den komplekse relasjonen mellom porøsitet, leirinnhold og P-bølgehastigheter på en enkel måte.

Contents

List of Symbols

β	Ratio of the clay volume to the sand volume
ν_{cl}	Poisson's ratio clay
ν_s	Poisson's ratio sand
ϕ	Total porosity
ϕ_{sh}	Critical porosity of shale
ϕ_s	Critical porosity of sand
ρ	Total density
ρ_{avg}	Average bulk density
ρ_c	Density of clay
ρ_s	Density of sand
ρ_w	Water density
c	The ratio of the volume of room dry shale (clay minerals and associated bound water and macroporosity) to the volume of room dry sand-shale mixture
C_{33clay}	Constant of the anisotropic clay
$C_{33\,Reuss}$	Reuss lower bound of the elastic modulus in the bedding-normal direction
$C_{33\,Voigt}$	Voigt upper bound of the elastic modulus in the bedding-normal direction
f_1	Volume fraction of first end-member
f_2	Volume fraction of second end-member

f_{cl}	Volumetric concentration of clay component
f_i	Volume fraction of ith phase
f_{sand}	Volume fraction of sand material
G_1	shear modulus first end-member
G_2	Shear modulus second end-member
G_{clay}	Shear modulus of of clay
G_{cl}	Shear modulus of clay grain pack
G_{EM}	Effective-medium shear modulus
G_{qtz}	Shear modulus of sand
K_1	Bulk modulus first end-member
K_2	Bulk modulus second end-member
K_b	Frame bulk moduli
K_{clay}	Bulk modulus of of clay
K_{cl}	Bulk modulus of clay grain pack
K_{EM}	Effective-medium bulk modulus
K_{fluid}	Bulk modulus of the pore fluid
K_{qtz}	Bulk modulus of sand
K_{sat}	Saturated bulk modulus
K_{solid}	Bulk modulus of solid material
L	Number of sand particles
l	Number of clay particles
M_i	Elastic modulus of ith phase
M_{qtz}	P-wave modulus of non-clay minerals
M_R	Reuss lower bound of effective modulus
M_V	Voigt upper bound of the elastic modulus

N	Number of phases
n_{cl}	Coordination number of the clay pack
n_s	Coordination number of the sand pack
P	Net stress
R	Radius of sand particles
r	Radius of clay particles
v_{clay}	Volumetric fraction of clay
$V_{pore-space}$	Pore-space volume of large grains packed together
V_p	P-wave velocity
V_{sand}	Total volume of a configuration consisting only of sand particles
V_{shale}	Total volume of a configuration consisting only of clay particles
w	Weighting factor

Chapter 1

Introduction

Obtaining accurate relations between velocity and porosity in porous rocks have been an important field of study in rock physics for decades. Information on these relations are of critical importance when seismic and/or sonic data are used to estimate porosity and other related properties (Nur et al., 1998). The information contained in velocity data can be used for lithology identification, fluid detection, porosity prediction, and for understanding compaction and burial history, among other things. P-waves are sensitive for several parameters, and when P-waves are the only information present, the primary effects have to be identified. To fathom the effects various geological features (e.g. lithology, fluid content, pressure scenarios) have on velocity and other rock-properties, rock-physics models may be constructed. Such models can provide a link between geologic and seismic parameters (Avseth et al., 2010), and each model has its benefits and limitations (Avseth et al., 2010).

There has been much focus on the relation between porosity and velocity (Wood, 1941; Wyllie et al., 1956; Raymer et al., 1980), and Marion et al. (1992) argues that studies that only account for the porosity-velocity relations fail to account for the scatter in the velocity-porosity data for unconsolidated material, arguing that this can be attributed to clay content. Marion et al. (1992) study the effect of porosity and clay content on compressional velocity in a binary system consisting of sand and clay. Their study is constructed by taking base in a geometrical model for a sand-clay mixture, as shown in Figure 1.1. The mixture is divided into two classes: a grain-supported regime consisting of sand and shaley sand, where the clay is dispersed in the sand pore space, and a matrix supported regime consisting of sandy shale and shale, where the sand grains are

dispersed in the clay matrix. Their findings show that there is a peak in velocities for sand-clay mixtures that is 20-30 percent higher than for pure sand or pure clay. Marion and Nur (1991) use a new method, called the Bound Averaging Method (BAM), to compute compressional and shear velocities, where they account for the effect of pore-filling elastic moduli. This is constructed using the Reuss lower bound and the Voigt upper bound.

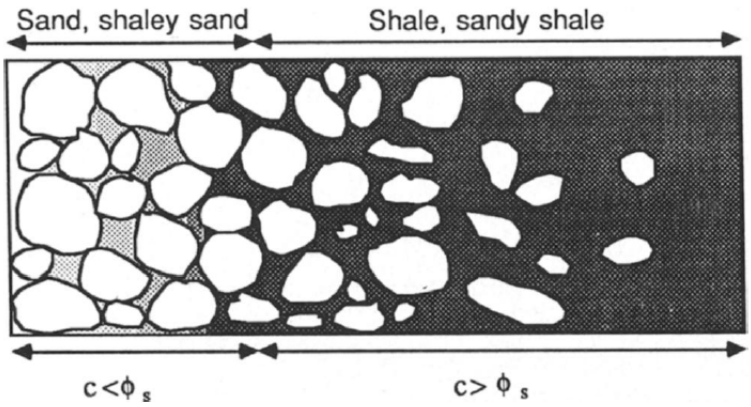

Figure 1.1: Geometry of the sand-clay mixture. The figure shows two sediment classes; sand and shaley sand, making up a grain-supported regime, and shale and sandy shaley, making up a matrix-supported regime. Figure courtesy: Marion et al. (1992).

Dvorkin and Nur (2002) presents a model which explains the deteriorating sorting in sands, but this model is only valid for grain-supported fabrics. Dvorkin and Gutierrez (2001b) presents a model that predicts the effect of textural sorting and variable framework composition and fabric on velocity and porosity, being valid for both grain- and mud-supported fabrics. This model takes base in a bimodal mixture consisting of large and small grains, where the large grains are the grain-supported fabric, and the small grains are the matrix-supported fabric. They argue that the theoretical relationships among seismic wave velocities, grain sorting, and composition suggested in the bimodal grain mixture model are essential when seismic or sonic data is used to predict reservoir quality in clastic rocks.

In this paper a new approach is introduced where the aim is to capture porosity and clay trends based solely on compressional velocities. The approach is constructed for a binary system consisting of a sand-clay mixture undergoing mechanical compaction. Two models are created, taking base in Dvorkin's Textural Sorting (Dvorkin and Gutierrez, 2001b) and the BAM model (Marion et al., 1992; Marion and Nur, 1991). They are modeled in relation to the geometry shown in Figure 1.1, going from a grain-supported

regime to a matrix-supported regime. This paper addresses the relation between clay content, porosity, and compressional velocities in such a geometry, and how these relations can be used for predictive purposes.

Chapter 2

Theory

Figure 1.1 shows the geometry of a sand-shale mixture that is divided into two domains: a grain-supported domain consisting of sand and shaley sand, and a matrix-supported domain consisting of sandy shale and shale. The first class represents the domain where the clay volume fraction, c, is less than the sand porosity, $c < \phi_{sand}$, and it represents a system in which the clay is dispersed in the pore space, i.e. a grain-supported regime. The second class represents the domain in which the clay volume fraction is higher than the sand porosity, $c > \phi_{sand}$, and represents a system in which the sand grains are dispersed in the clay matrix, i.e. a matrix-supported regime. The porosity will decrease as the clay content increases for the grain-supported regime, but as the model transitions into the matrix supported regime, the sand will be dispersed in the clay matrix, causing the porosity to increase with increasing clay content (Marion et al., 1992).

Marion et al. (1992) creates a method to predict porosities for sand-clay mixtures, where the porosity will change as a function of clay content. They further use this relationship between porosity and clay content to predict compressional velocities for the binary system.

Dvorkin and Gutierrez (2001b) creates a model that predicts the effect of textural sorting and variable composition and fabric on velocity and porosity. The model is based on a bimodal mixture consisting of small and large grains, and Dvorkin and Gutierrez (2001b) use the relationship between the geometry of the small and large grains to create a model to explain the relation between porosity, clay content, and velocity.

In this section the two models are presented, and how they can be used to model poros-

ity, clay content, and velocity in a binary system consisting of a sand-clay mixture is described. The models are explained in relation to the geometry shown in Figure 1.1, explaining how the models transition from the grain-supported regime to the matrix-supported regime.

2.1 Dvorkin's Textural Sorting

Dvorkin and Gutierrez (2001b) propose a model that predicts the effect of textural sorting and variable composition and fabric on velocity and porosity. Porosity, mineralogy, pressure, texture, fabric, and pore fluid modulus is linked to the elastic rock properties in this model. The model creates theoretical relationships that are essential in predicting reservoir quality in clastic rocks by using seismic or sonic data (Dvorkin and Gutierrez, 2001b).

2.1.1 Porosity Model for a Bimodal Grain Mixture

To calculate porosity, Dvorkin and Gutierrez (2001b) take base in a bimodal mixture of elastic spheres or perfectly rounded grains, and assume that there are only two grain sizes present in the mixture; large and small grains. The diameter of the large grains is assumed to be much larger than the diameter of the small grains, and, depending on the volumetric fraction of the two grain sizes, various configurations are possible (Dvorkin and Gutierrez, 2001b). Figure 2.1 shows a schematic illustration of this system, where large grains are presented in (a), and by moving rightwards, smaller grains slowly start to fill the pore space of the large grains. As the volume of the small grains increases, it will expand the lattice of the large grains, eventually resulting in a configuration only consisting of small grains, as shown in figure (e). This is a dispersed form of mixing, and it is the most compact way of mixing grains of different grain sizes (Dvorkin and Gutierrez, 2001a). As the aim of this paper is to predict porosity and clay content based on velocity, the model is alternated to account for a mixture specifically consisting of sand (large grain pack) and clay (small grain pack).

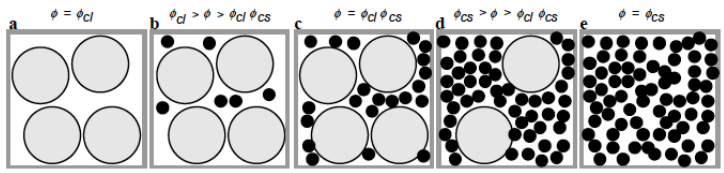

Figure 2.1: Geometry of the bimodal grain mixture. The porosity reduces as the sorting deteriorates, and increases again as only the small grains make up the mixture. ϕ_{cl} is equivalent with ϕ_s, and ϕ_{cs} is equivalent with ϕ_{sh}. Figure courtesy: Dvorkin and Gutierrez (2001b).

The volume of the clay and sand grains can be calculated based on their radii and critical porosity. The total volume of a configuration consisting only of clay particles with

radius r at critical porosity ϕ_{sh} is (Dvorkin and Gutierrez, 2001b):

$$V_{shale} = \frac{4}{3}\frac{\pi r^3 l}{1-\phi_{sh}} \tag{2.1}$$

and for a configuration consisting only of sand particles with radius R at critical porosity ϕ_s the total volume is (Dvorkin and Gutierrez, 2001b):

$$V_{sand} = \frac{4}{3}\frac{\pi R^3 L}{1-\phi_s} \tag{2.2}$$

where L and l denotes the number of sand and clay particles, respectively, in a representative volume (Dvorkin and Gutierrez, 2001b).

The pore-space volume of the large grains packed together is Dvorkin and Gutierrez (2001b):

$$V_{pore-space} = \frac{4}{3}\frac{\phi_s \pi R^3 L}{1-\phi_s} \tag{2.3}$$

To calculate the porosity in the different configurations seen in Figure 2.1, Dvorkin and Gutierrez (2001b) use the ratio of the clay volume to the sand volume, β:

$$\beta \equiv (\frac{r^3 l}{1-\phi_{sh}})/(\frac{R^3 L}{1-\phi_s}) \tag{2.4}$$

If $\beta = 0$, the mixture will only consist of clean sand, causing the porosity to be equal to the porosity of the sand, i.e. $\phi = \phi_s$, as is the case for (a) in Figure 2.1. If β is smaller than the sand porosity, the clay particles can be filled inside the pore space of the sand (Dvorkin and Gutierrez, 2001b), as is seen in (b) in Figure 2.1. The total porosity of the mixture will then be $\phi = \phi_s - \beta(1-\phi_{sh})$, causing the porosity of the sand-clay mixture to decrease, as can be seen in Figure 2.2(a).

When $\beta = \phi_s$, the mixture is equivalent to that of (c) in Figure 2.1, and the sand grains are in contact with each other (Dvorkin and Gutierrez, 2001b). This point separates

the two different domains; the grain-supported (shaley sand) and the matrix supported (sandy shale) domain (Dvorkin and Gutierrez, 2001a). This causes the porosity to be calculated as the product of the porosity of the sand and the clay, i.e. $\phi = \phi_s \phi_{sh}$.

When $\beta > \phi_s$, the mixture will have changed from a grain-supported regime to a matrix-supported regime, and the sand particles are now in suspension (Dvorkin and Gutierrez, 2001b), as seen in (d) in Figure 2.1. The porosity can be calculated as follows:

$$\phi = \frac{\phi_{sh}}{1 + (1 - \phi_s)/\beta} \tag{2.5}$$

When $\beta = \infty$, only the clay particles will be present in the mixture, thus causing the porosity to be equal to the shale porosity, i.e. $\phi = \phi_{sh}$ (Dvorkin and Gutierrez, 2001b). Figure 2.2(a) shows how the porosity changes as β increases, clearly showing that the total porosity approaches the critical porosity for the clay grain pack as β approaches ∞.

To summarize (Dvorkin and Gutierrez, 2001b):

$$\phi = \phi_s - \beta(1 - \phi_{sh}) \Leftarrow \beta < \phi_s \tag{2.6}$$

$$\phi = \phi_s \phi_{sh} \Leftarrow \beta = \phi_s \tag{2.7}$$

$$\phi = \frac{\phi_{sh}}{1 + (1 - \phi_s)/\beta} \Leftarrow \beta > \phi_s \tag{2.8}$$

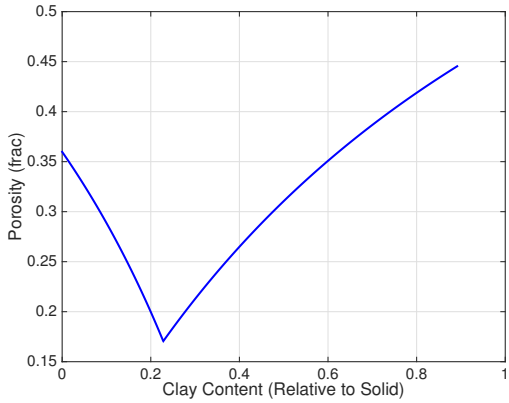

((a)) The figure illustrates how the porosity changes as β increases. The porosity will begin to decrease as the the pore space is filled with clay particles, but starts to increase when β equals the sand porosity. As β increases, the total porosity will reach the value of the shale porosity. The critical porosity of the sand is here 0.3598 and 0.4739 for the shale.

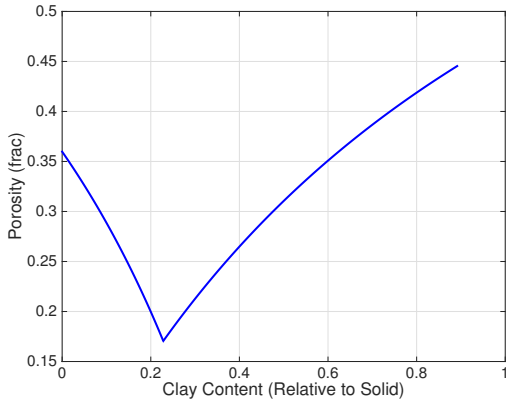

((b)) To compare the model to lab data, we have to create a function that determines the porosity as a function of clay content. The figure shows how the porosity changes as the clay content increases. The porosity decreases with increasing clay content for the grain-supported regime, but the porosity increases with increasing clay content for the matrix-supported regime.

Figure 2.2: Porosity as a function of β and clay content.

2.1.2 Elasticity of a Bimodal Grain Mixture

The elastic moduli of the bimodal grain mixture is found by using the same principles as explained above. If $\beta \geqslant \phi_s$, the sand grains are in suspension (Figure 2.1e). Assuming that the sand has a much larger elastic moduli than the clay, the clay will act as the soft grain pack enveloping the stiffer grain pack of sand (Dvorkin and Gutierrez, 2001b). By assuming this, one can model the elastic moduli of the mixture by using the lower Hashin-Shtrikman (Hashin and Shtrikman, 1963), where the clay is defined as the soft component and the sand is defined as the stiff component. Following the same principals explained in the section above, the volumetric concentration of the clay component is (Dvorkin and Gutierrez, 2001b):

$$f_{cl} = \frac{1}{1 + (1 - \phi_s)/\beta} \tag{2.9}$$

The effective-medium elastic moduli of the dry component will then be as follows (Dvorkin and Gutierrez, 2001b):

$$K_{EM} = [\frac{f_{cl}}{K_{cl} + \frac{4}{3}G_{cl}} + \frac{1 - f_{cl}}{K_{qtz} + \frac{4}{3}G_{cl}}]^{-1} - \frac{4}{3}G_{cl} \tag{2.10}$$

$$G_{EM} = [\frac{f_{cl}}{G_{cl} + Z_{cl}} + \frac{1 - f_{cl}}{G_{qtz} + Z_{cl}}]^{-1} - Z_{cl} \tag{2.11}$$

$$Z_{cl} = \frac{G_{cl}}{6}\frac{9K_{cl} + 8G_{cl}}{K_{cl} + 2G_{cl}} \tag{2.12}$$

where K_{qtz} and G_{qtz} are the bulk and shear moduli of the sand, respectively, and K_{cl} and G_{cl} are the bulk and shear moduli of the clay grain pack, respectively.

Although the clay particles are more elongated than spherical, for simplicity, the clay particles are approximated as a dense pack of identical elastic spheres. By doing so, the elastic moduli can be calculated by using the Hertz-Mindlin contact theory (Mindlin, 1949):

$$K_{cl} = [\frac{n_{cl}^2(1-\phi_{sh})^2 G_{clay}^2}{18\pi^2(1-\nu_{cl})^2} P]^{\frac{1}{3}} \tag{2.13}$$

$$G_{cl} = \frac{5-4\nu_{cl}}{5(2-\nu_{cl})} [\frac{3n_{cl}^2(1-\phi_{sh})^2 G_{clay}^2}{2\pi^2(1-\nu_{cl})^2} P]^{\frac{1}{3}} \tag{2.14}$$

$$\nu_{cl} = \frac{1}{2}(\frac{K_{clay}}{G_{clay}} - \frac{2}{3})/(\frac{K_{clay}}{G_{clay}} + \frac{1}{3}) \tag{2.15}$$

where the coordination number for the clay pack, n_{cl}, is found by (Mavko et al., 2009):

$$n_{cl} = 24e^{-2.547\phi_{sh}} - 0.373 \tag{2.16}$$

where K_{clay} and G_{clay} are the bulk and shear moduli of the clay, respectively, and P is the net stress.

If $\beta \leq \phi_{sh}$, there are two elastic end members consisting of $\beta = 0$ and $\beta = \phi_s$. By assuming that the sand grains are identical spheres, the first end-member can be calculated using the Hertz-Mindlin contact theory (Mindlin, 1949) with bulk modulus K_{qtz}, shear modulus G_{qtz}, and coordination number n_s. The bulk modulus K_1 and shear modulus G_1 will then be:

$$K_1 = [\frac{n_s^2(1-\phi_s)^2 G_{qtz}^2}{18\pi^2(1-\nu_s)^2} P]^{\frac{1}{3}} \tag{2.17}$$

$$G_1 = \frac{5-4\nu_s}{5(2-\nu_s)} [\frac{3n_s^2(1-\phi_s)^2 G_{qtz}^2}{2\pi^2(1-\nu_s)^2} P]^{\frac{1}{3}} \tag{2.18}$$

$$\nu_s = \frac{1}{2}(\frac{K_{qtz}}{G_{qtz}} - \frac{2}{3})/(\frac{K_{qtz}}{G_{qtz}} + \frac{1}{3}) \tag{2.19}$$

where the coordination number for the sand pack, n_s, is found by (Mavko et al., 2009):

$$n_s = 24e^{-2.547\phi_s} - 0.373 \tag{2.20}$$

The elastic moduli of the second end-member at $\beta = \phi_s$, are given by:

$$K_2 = [\frac{\phi_s}{K_{cl} + \frac{4}{3}G_{cl}} + \frac{1-\phi_s}{K_{qtz} + \frac{4}{3}G_{cl}}]^{-1} - \frac{4}{3}G_{cl} \tag{2.21}$$

$$G_2 = [\frac{\phi_s}{G_{cl} + Z_{cl}} + \frac{1-\phi_s}{G_{qtz} + Z_{cl}}]^{-1} - Z_{cl} \tag{2.22}$$

$$Z_{cl} = \frac{G_{cl}}{6}\frac{9K_{cl} + 8G_{cl}}{K_{cl} + 2G_{cl}} \tag{2.23}$$

To find the configuration shown in Figure 2.1, frame (b), it can be assumed that adding the configurations shown in frame (a) and frame (c) will result in the numbers of sand and clay particles in the configuration in frame (b) in Figure 2.1.

Defining the volume fraction of the first end member as f_1 and that of the second end-member as $f_2 = 1 - f_1$, the number of clay particles in a unit volume of the composite will be (Dvorkin and Gutierrez, 2001b):

$$l = \frac{f_2\phi_s(1-\phi_{sh})}{\frac{4}{3}\pi r^3} \tag{2.24}$$

and the number of the large grains is:

$$L = \frac{1-\phi_s}{\frac{4}{3}\pi R^3} \tag{2.25}$$

β can then be expressed as:

$$\beta \equiv (\frac{r^3 l}{1-\phi_{sh}})/(\frac{R^3 L}{1-\phi_s}) = f_2\phi_s \tag{2.26}$$

And this results in:

$$f_2 = \beta/\phi_s \tag{2.27}$$

and,

$$f_1 = 1 - f_2 \tag{2.28}$$

By assuming that the first end-member is softer than the second and connecting the two points by Hashin-Shtrikman, the elastic moduli of the composite's dry frame will be (Dvorkin and Gutierrez, 2001b):

$$K_{EM} = [\frac{f_1}{K_1 + \frac{4}{3}G_1} + \frac{f_2}{K_2 + \frac{4}{3}G_1}]^{-1} - \frac{4}{3}G_1 \tag{2.29}$$

$$G_{EM} = [\frac{f_1}{G_1 + Z_1} + \frac{f_2}{G_2 + Z_1}]^{-1} - Z_1 \tag{2.30}$$

$$Z_1 = \frac{G_1}{6}\frac{9K_1 + 8G_1}{K_1 + 2G_1} \tag{2.31}$$

with the bulk and shear moduli K_1 and G_1, and K_2 and G_2, respectively, and volume fractions f_1 and f_2, respectively (Dvorkin and Gutierrez, 2001b).

To find the saturated bulk modulus of the composite, Gassmann's equation is applied (Dvorkin and Gutierrez, 2001b):

$$K_{sat} = K_{Solid}\frac{\phi K_{EM} - (1+\phi)K_{Fluid}K_{EM}/K_{Solid} + K_{fluid}}{(1-\phi)K_{Fluid} + \phi K_{solid} - K_{Fluid}K_{EM}/K_{Solid}} \tag{2.32}$$

where K_{fluid} is the bulk modulus of the pore fluid and K_{solid} can be calculated by mixing the material of the sand with that of the clay, using Hill's average.

The volume fraction f_{sand} of the sand material in the entire solid phase of the composite is calculated as follows (Dvorkin and Gutierrez, 2001b):

$$f_{sand} = \frac{R^3 L}{R^3 L + r^3 l} = \frac{1}{1 + \frac{r^3 l}{R^3 L}} = \frac{1}{1 + \frac{\beta(1-\phi_{sh})}{1-\phi_{sand}}} \tag{2.33}$$

with Hill's average as (Dvorkin and Gutierrez, 2001b; Mavko et al., 2009):

$$K_{solid} = \frac{1}{2}[f_{sand} K_{qtz} + (1 - f_{sand}) K_{clay} + (\frac{f_{sand}}{K_{qtz}} + \frac{1 - f_{sand}}{K_{clay}})^{-1}] \tag{2.34}$$

The velocity is then calculated as:

$$V_p = \sqrt{\frac{K_{sat} + \frac{4}{3} G_{EM}(\beta \leq \phi_s)}{\rho}} \tag{2.35}$$

for $\beta \leq \phi_s$, and for $\beta \geq \phi_s$:

$$V_p = \sqrt{\frac{K_{sat} + \frac{4}{3} G_{EM}(\beta \geq \phi_s)}{\rho}} \tag{2.36}$$

where ρ is calculated as:

$$\rho = (1 - \phi)\rho_{avg} + \phi_t \rho_w \tag{2.37}$$

where ρ_{avg} is the average bulk density, ρ_w is the water density, and ϕ is the total porosity.

2.2 The Modified BAM

2.2.1 Porosity in Sand-Clay Mixtures

Marion et al. (1992) propose a method for determining porosities in sand-clay mixtures. The model is based on the difference in the packing of the particles present, and explains how this can be used to calculate porosities and compressional velocities. As can be seen from Figure 1.1, the model explains the transition from sand and shaly sand to sandy shale and shale, where the clay volume fraction, c, increases as the mixture transitions into pure shale. Here, c is defined as "the ratio of the volume of room dry shale (clay minerals and associated bound water and macroporosity) to the volume of room dry sand-shale mixture" (Marion et al., 1992).

When the clay volume fraction is less than the sand porosity, c<ϕ_s, Marion et al. (1992) states that the clay particles will fill the pore space of the sand, which causes the porosity of the binary system to decrese linearly with an increase in the clay volume:

$$\phi = \phi_s - c(1 - \phi_{sh}) \tag{2.38}$$

When the clay volume fraction equals the sand porosity, c=ϕ_s, Marion et al. (1992) states that the shaley material will fill the pore space of the sand entirely, thus causing the porosity to be equal to the product of the sand and shale porosity:

$$\phi = \phi_s \phi_{sh} \tag{2.39}$$

When the clay volume fraction exceeds the sand porosity, c>ϕ_s, the clay will expand the sand lattice, causing the sand grains to disconnect, and the sand grains will be replaced by porous shaley material. The porosity will then increase linearly as the clay volume increases(Marion et al., 1992):

$$\phi = c\phi_{sh} \tag{2.40}$$

The densities will also change as the clay content and porosity change, and Marion et al. (1992) propose following equations:

$$\rho = (1-\phi_s)\rho_s + c(1-\phi_{sh})\rho_c + (\phi_s - c(1-\phi_{sh}))\rho_w \tag{2.41}$$

for $c < \phi_s$, and for $c > \phi_s$:

$$\rho = (1-c)\rho_s + c(1-\phi_{sh})\rho_c + c\phi_{sh}\rho_w \tag{2.42}$$

where ρ_s is the density of the sand, ρ_c is the density of the clay, and ρ_w is the water density.

The porosities of sand and shale will change as they are measured under different pressures. The porosity model thus accounts for mechanical compaction.

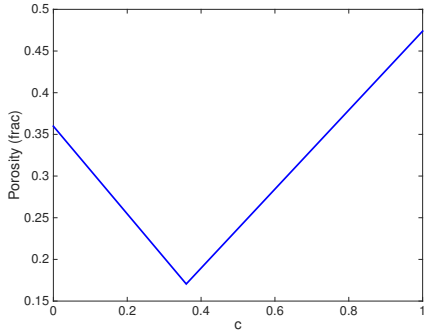

((a)) Porosity as a function of c. The porosity decreases with increasing c for the grain-supported regime, but starts to increase with increasing c in the matrix-supported regime.

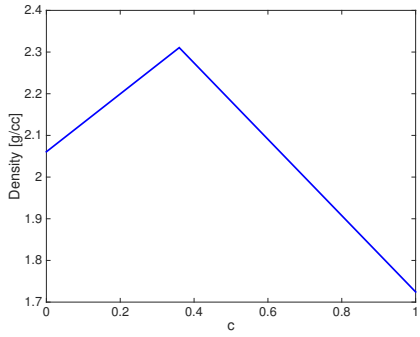

((b)) Density as a function of c. The density will increase as c increases in the grain-supported regime, but starts to decrease with increasing c as the mixture transitions into the matrix-supported regime.

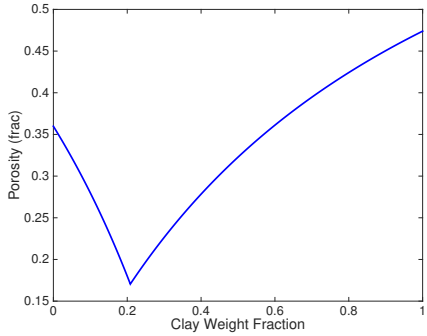

((c)) Porosity as a function of clay weight fraction. The porosity decreases with increasing clay content for the grain-supported regime, but starts to increase with increasing clay content in the matrix-supported regime.

Figure 2.3: Density and porosity as a function of c and clay porosity as a function of clay weight fraction. All figures represent the model at a net stress of 9 MPa, with $\phi_s = 0.3598$ and $\phi_{sh} = 4739$.

2.2.2 The Bound Averaging Method

The compressional velocities can be found using the BAM proposed by Marion and Nur (1991).

The BAM tries to estimate the elastic moduli of the rock given its porosity and the elastic moduli of its constituent mineral and fluid phases (Marion and Nur, 1991). They create upper and lower bounds by Voigt and Reuss, respectively. The Reuss lower bound gives the ratio of the average stress to the average strain when all constituents are assumed to have the same stress, and it is also referred to as the iso-stress average (Mavko et al., 2009; Marion and Nur, 1991). It describes the effective moduli of a suspension of solid grains in a fluid, and when all constituents are gases or liquids, or both, with a shear moduli of zero, the Reuss average will give the exact effective moduli of the mixture (Mavko et al., 2009). The Reuss lower bound of the effective modulus, M_R, of N phases is (Mavko et al., 2009):

$$\frac{1}{M_R} = \sum_{i=1}^{N} \frac{f_i}{M_i} \tag{2.43}$$

where f_i is the volume fraction of the ith phase and M_i is the elastic modulus of the ith phase (Mavko et al., 2009).

The Voigt upper bound gives the ratio of the average stress to the average strain when all constituents are assumed to have the same strain, and it is also referred to as the iso-strain average (Mavko et al., 2009; Marion and Nur, 1991). Except for a single phase end-member, real isotropic mixutres can never be as stiff as the Voigt bound. The Voigt upper bound of the elastic modulus, M_V, of N phases is (Mavko et al., 2009):

$$M_V = \sum_{i=1}^{N} f_i M_i \tag{2.44}$$

where f_i is the volume fraction of the ith phase and M_i is the elastic modulus of the ith phase (Mavko et al., 2009). Both bounds presuppose that each constituent is isotropic, linear, and elastic (Mavko et al., 2009; Avseth et al., 2010).

Using the theory of the Reuss and Voigt bounds, Marion and Nur (1991) assume that the elastic modulus M of a rock may be expressed as a weighted arithmetic average be-

tween the upper and lower bounds, M^+ and M^-, respectively (Marion and Nur, 1991):

$$M = M^- + w(M^+ - M^-) \tag{2.45}$$

where the weighting factor, w, ranges from 0 to 1, and is a measure of the average pore space stiffness (Marion and Nur, 1991). They further assume that w is unaffected by the type of pore filling, and for a given rock, it is a constant for a given elastic modulus (Marion and Nur, 1991). It is, however, worth noting that the weighting factor is not necessarily identical for all elastic moduli of a given rock (Marion and Nur, 1991).

The velocities can then be calculated as (Marion and Nur, 1991):

$$V = \sqrt{\frac{M}{\rho}} \tag{2.46}$$

with densities calculated as in equation 2.41 and 2.42.

Knowing that most clays are anisotropic (Vernik and Kachanov, 2010; Wang, 2001), an extension of this is to use the Reuss and Voigt bounds to account for anisotropy. This can be modeled by constructing upper and lower bounds of the elastic constant for compressional velocity in the bedding-normal direction. Rearranging the equations for the the Reuss and Voigt bounds to account for anisotropy thus yields:

$$C_{33Reuss} = \left(\frac{v_{clay}}{C_{33clay}} + \frac{v_{sand}}{M_{qtz}} + \frac{\phi_{tot}}{K_b} \right)^{-1} \tag{2.47}$$

$$C_{33Voigt} = v_{clay} C_{33clay} + v_{sand} M_{qtz} + \phi_{tot} K_b \tag{2.48}$$

where v_{clay} is the volumetric fraction of clay in the rock, C_{33clay} is the constant of the anisotropic clay, M_{qtz} is the P-wave modulus of the remaining minerals, ϕ_{tot} is the total porosity as calculated from Marion (Marion et al., 1992), and K_b is the frame bulk moduli.

$C_{33Reuss}$ and $C_{33Voigt}$ are inserted into equation 2.45, where they replace M^- and M^+,

respectively. Further, w is an iso-stress analogue for Reuss, causing us to assume that this parameter will increase linearly with depth/increasing pressure. The compressional velocity is then calculated as:

$$V_p = \sqrt{\frac{C_{33}}{\rho}} \tag{2.49}$$

with C_{33} being:

$$C_{33} = C_{33Reuss} + w(C_{33Voigt} - C_{33Reuss}) \tag{2.50}$$

and where ρ is calculated as in equations 2.41 and 2.42.

Chapter 3

Data

3.1 Lab Data

The modified BAM and Dvorkin's Textural Sorting have been compared to lab data presented in Marion et al. (1992). The data have been digitalized, and Figure 3.1 and Figure 3.2 shows the results of the lab measurements that are conducted by Marion et al. (1992).

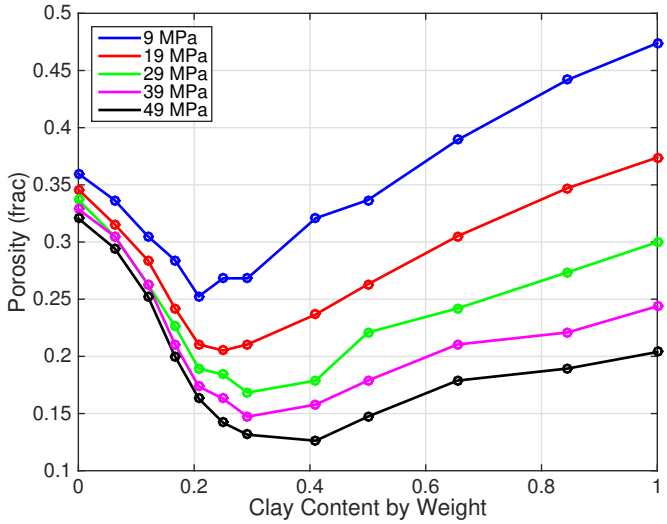

Figure 3.1: Porosity as a function of clay weight fraction. The values are obtained from lab experiment. Data courtesy: Marion et al. (1992).

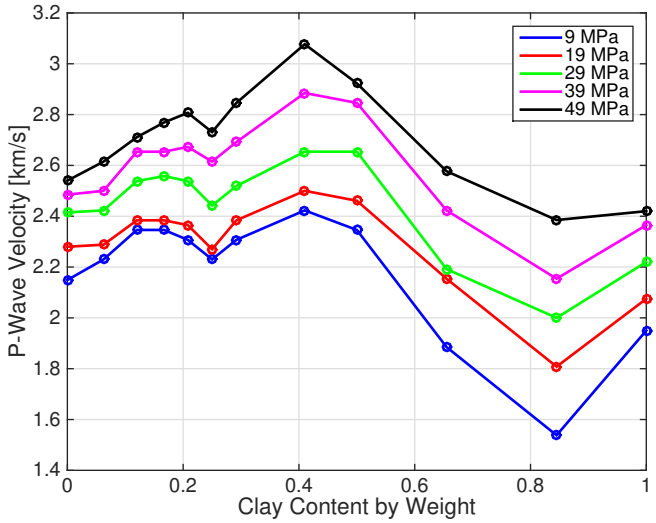

Figure 3.2: Velocity as a function of clay weight fraction. The values are obtained from lab experiment. Data courtesy: Marion et al. (1992).

3.2 Well data

3.2.1 Well 6608/10-3: The Norwegian Sea

The models are tested on well 6608/10-3 located in the Norwegian Sea, the Norne field. The well location is at 66° 2' 6.66" N, 8° 4' 57.97" E (NPD, a). From this well wireline velocity, density, and gamma ray are retrieved and used to obtain porosity and volumetric clay content.

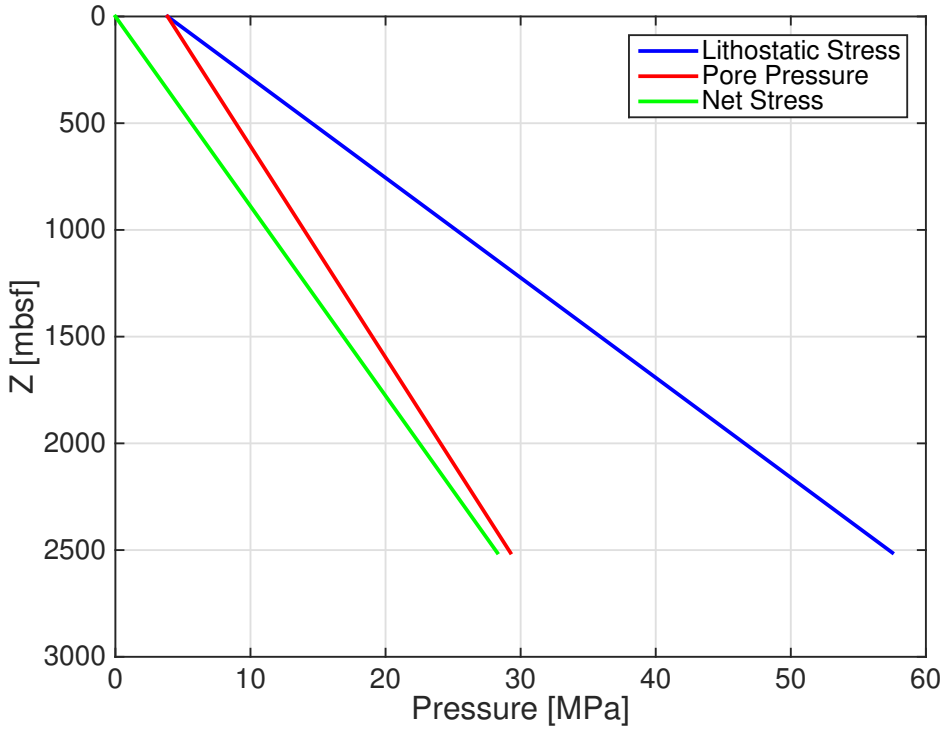

Figure 3.3: Pressure trends in well 6608/10-3 estimated from the well log.

3.2.2 Well 34/7-1: The North Sea

The models are also tested on well 34/7-1 in the North Sea, the Snorre field. The well location is at 61° 28' 21.8" N, 2° 13' 25.55" E (NPD, b). From this well wireline velocity, density, and gamma ray are retrieved and used to obtain porosity and volumetric clay content.

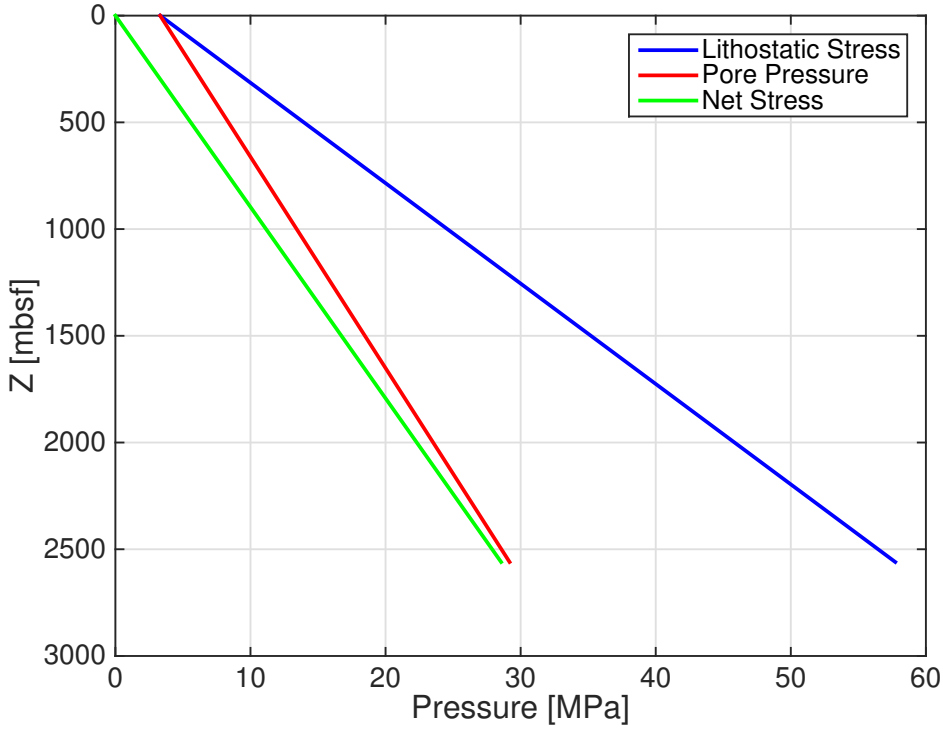

Figure 3.4: Pressure trends in well 34/7-1 estimated from the well log.

3.2.3 Well 33/5-2: The North Sea

The third well the models are tested on is well 33/5-2 in the North Sea. The well location is at 61° 39' 47.14" N, 1° 37' 17.4" E (NPD, c). From this well wireline velocity, density, and gamma ray are retrieved and used to obtain porosity and volumetric clay content.

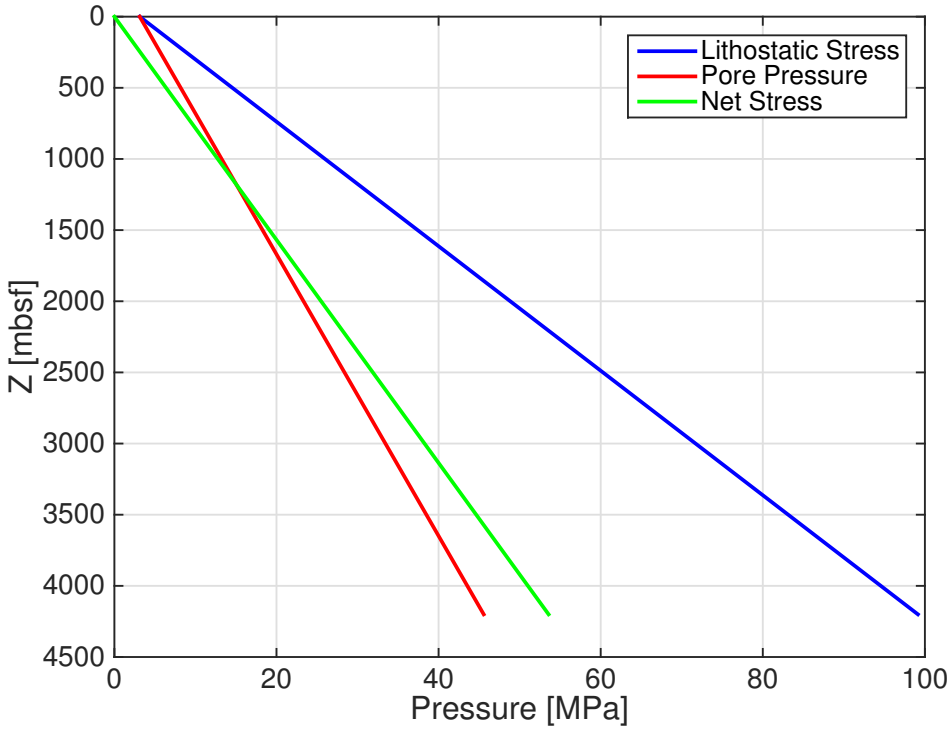

Figure 3.5: Pressure trends in well 33/5-2 estimated from the well log.

3.3 Clay Trends

The two figures below show the distribution of different clay minerals in well 34/7-1 in the North Sea and well 6405/7-1 in the Norwegian Sea. The amount of smectite increases when entering the Hordaland Group and Rogaland Group. High smectite content correlates with low velocities and is considered to be the most important factor controlling velocity variations with depth in basins where smectitic clays are undergoing mechanical compaction (Marcussen et al., 2009). Smectite has low compressibility and very low permeability (Peltonen et al., 2008), and this favors overpressure generation which further prevents mechanical compaction (Storvoll et al., 2005). Thus, overpressure may be identified in well logs as a deviation from a normal compaction curve with increasing velocities with depth (Marcussen et al., 2009).

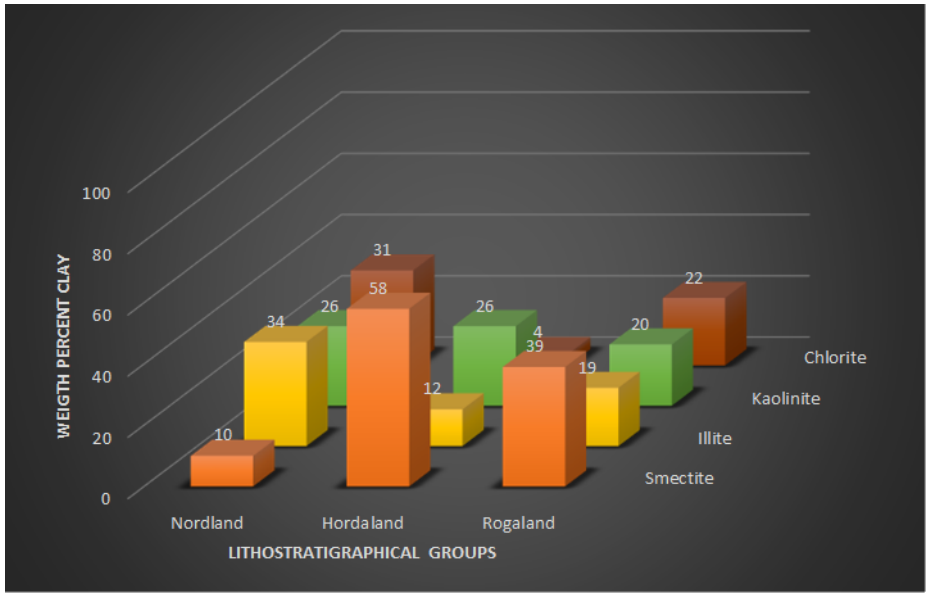

Figure 3.6: The figure shows the weight percent of different clays in well 34/7-1. The amount of smectite is highly increasing in the Hordaland Group and Rogaland Group. Data courtesy: Marcussen et al. (2009).

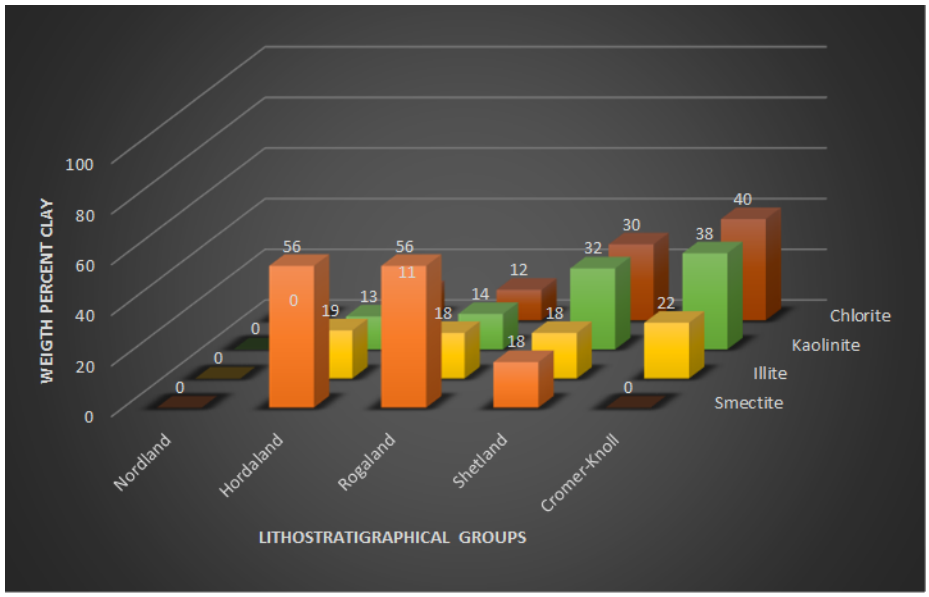

Figure 3.7: The figure shows the weight percent of different clays in well 6405/7-1. The amount of smectite is highly increasing in the Hordaland Group and Rogaland Group. Data courtesy: Peltonen et al. (2008).

Chapter 4

Methodology

In the above sections, it has been described how the modified BAM and Dvorkin's Textural Sorting conceptualize the relationship between porosity and clay content in a binary system. How theses relations can be used to predict porosity and clay content from compressional velocities will be described in the following section.

4.1 The Modified BAM and Dvorkin's Textural Sorting: Validity of Assumptions

The modified BAM and Dvorkin's Textural Sorting both conceptualize a binary system consisting of sand and clay, where the elastic moduli is calculated going from a grain-supported regime (starting at clean sand) to a matrix-supported regime (ending at clean shale). Both models describe a sand-clay mixture, but they have some assumptions, weaknesses, and strengths that differ from each other, which will be presented here.

One of the assumptions underlying Dvorkin's model is that the mixture is isotropic and consists of spherical grains. It is worth noting that this assumption is not necessarily correct, as clays exhibit a more elongated shape rather than a spherical shape, causing the packing of the particles to differ from that of spherical grains. It is also known that most clays are anisotropic (Vernik and Kachanov, 2010; Wang, 2001), and by assuming isotropy, the validity of the model is weakened for the case that is being studied. However, the concept remains the same, and it provides a conceptually easy way to model

sand-clay mixtures, along with being based on acknowledged rock-physics theory.

The effect of mechanical compaction in Dvorkin's model is taken into account by the pressure-term in equations 2.13, 2.14, 2.17, and 2.18, as well as it is given by the critical porosity terms for sand and clay in the same equations, as well as in equations 2.21 and 2.22. These parameters will change as the model is used for different depths/pressures, corresponding to the mechanical compaction that the sand-clay mixture is undergoing. Having an explicit pressure-term in this model is an advantage, making it easy to model the effect of pressure trends.

Despite the fact that Dvorkin's model does not account for anisotropy, nor acknowledges the shape of clay minerals, the simple conceptualization and acknowledgement of this model justifies its application.

The modified BAM differs from Dvorkin's Textural Sorting by introducing an anisotropic elastic constant for compressional velocity in the bedding-normal direction, given by equation 2.47 and 2.48, thus accounting for anisotropy in the clay. One of the assumptions underlying the porosity model used in the modified BAM, is that the sand lattice will not be disturbed as the pore space is filled with clay. Likewise, it is also assumed that the sand grains will not disturb the shale packing. According to Marion et al. (1992), this assumption is practically only valid when the clay content is either very high or very low. As the clay fills the pore space of the sand, the sand lattice will expand, resulting in higher porosities for the shaley sand. Furthermore, when the sand lattice expands, the pore space will be filled with more clay, shifting the minimum porosity point towards higher clay contents. According to Marion et al. (1992), this model can be seen as a lower bound for porosity. This indicates that the porosity model does not provide accurate porosity estimations for the transition between the grain-supported regime and the matrix-supported regime, but it should provide accurate estimations for clean sand and clean shale. It should therefore be assumed to find deviations in the transition between the grain-supported regime and the matrix-supported regime.

The effect of mechanical compaction for the modified BAM is taken into account by the critical porosity term for the sand and shale, which will vary according to changes in the net stress. Also, w, acting as an iso-stress analogue for Reuss, will increase with increasing depth/pressure, thus be a parameter controlling the pressure conditions, and in that way account for mechanical compaction.

As with Dvorkin's model, the modified BAM conceptualizes a complex problem in an easy way, creating a model that explains how the constituents of the mixture affects the

porosity. The anisotropy-term in the modified BAM makes it a reasonable fit to model sand-clay mixtures.

The two models are similar in the way they conceptualize the relationship between porosity and clay content in sand-clay mixtures. Dvorkin's biggest advantage lies in the acknowledgement of the rock physics theory underlying the model and its simplicity of modeling effects of pressure, while the modified BAM is strengthened by introducing an anisotropic elastic constant. It should be assumed to find differences in the results for the two models, and the findings will be discussed in the Results chapter.

4.2 Calibrating the Models to Lab Data

To be able to compare the results of the models to the lab data presented in Marion et al. (1992), the clay volume fraction in the modified BAM needs to be converted into clay weight fraction (Marion et al., 1992):

$$w_c = \frac{c(1-\phi_{sh})\rho_c}{c(1-\phi_{sh})\rho_c + (1-\phi_s)\rho_s} \tag{4.1}$$

for $c < \phi_s$, and for $c > \phi_s$:

$$w_c = \frac{c(1-\phi_{sh})\rho_c}{c(1-\phi_{sh})\rho_c + (1-c)\rho_s} \tag{4.2}$$

Likewise, it is necessary to calculate the clay content relative to the solid phase for Dvorkin's model. As the volume fraction of the sand in the solid phase of the mixture is given by f_l, the clay content in the solid phase will be given by:

$$V_{cl,solid} = 1 - f_l \tag{4.3}$$

The models need to be calibrated to account for the same conditions as the lab data is subject to. The sand-clay mixture is assumed to be fully water saturated, and it is modeled with confining pressures of 10 MPa, 20 MPa, 30 MPa, 40 MPa, and 50 MPa. The pore pressure is held constant at 1 MPa for all confining pressures, thus yielding net stresses of 9 MPa, 19 MPa, 29 MPa, 39 MPa, and 49 MPA. The modeled results are compared to the data presented in the section above; Figure 3.1 and Figure 3.2. The corresponding porosities of sand and shale at these pressures are given in Table 4.1.

Further, as w is an iso-stress analogue for Reuss, this parameter will change with depth. The values used for w are listed in Table 5.1 in the Results chapter.

σ'	ϕ_s	ϕ_{sh}
9 MPa	0.3598	0.4739
19 MPa	0.3459	0.3739
29 MPa	0.3368	0.2999
39 MPa	0.3287	0.2438
49 MPa	0.3206	0.2038

Table 4.1: Values for ϕ_s and ϕ_{sh} at the corresponding net stresses. Data courtesy: Marion et al. (1992).

4.3 Calibrating the Models to Well Data

To resemble the environment in which the well data are retrieved, the sand- and shale porosities are calibrated, where well 6608/10-3 is used as calibration well for the two models. The calibration is carried out by plotting porosity and clay content from the two models with porosity and clay content from the well data at net stresses of 9, 19, and 27 MPa. The well data plotted is retrieved from the depth intervals corresponding to these net stresses, $\pm 50m$. To fit the models with the well data, the sand- and shale-porosities are changed in such a way that they intersect with the well data. These results are found in the next chapter, in Figure 5.6, 5.8, and 5.10. The porosities at the corresponding net stresses are listed in Table 5.2.

For wells 34/7-1 and 33/5-2, the sand- and shale-porosities used in the modeling is based on the calibration of well 6608/10-3, along with information from the sonic velocity log. The highest porosities are assigned to intervals displaying low velocities.

When modeling the modified BAM, w has been used to account for changing pressure. All values used for porosities and w are found in the Appendix.

4.4 Predicting Porosity and Clay Content from Compressional Velocities

To retrieve the estimated porosity and clay content from the two models at a given velocity, the velocities from the well log at given net stresses are used. When running the models, these given velocities are inserted, and the corresponding estimations of clay content and porosity values at these velocities at given net stresses are obtained. For each model, two possible porosities and two possible clay content values will be obtained, corresponding to two porosity-clay content pairs. This is illustrated in Figures 4.1 and 4.2. If the velocities are low, the velocity will only intersect the model in one point, giving only one porosity-clay content pair. The estimated values are then plotted with the well data for given depths/net stresses.

The sand-clay mixture is assumed to be fully water saturated, and the modeling is carried out at net stresses ranging from 0 to 28 MPa, with a steplength of 1 MPa, for wells 6608/10-3 and 34/7-1. For well 33/5-2 the modeling is carried out for net stresses ranging from 0 to 50 MPa.

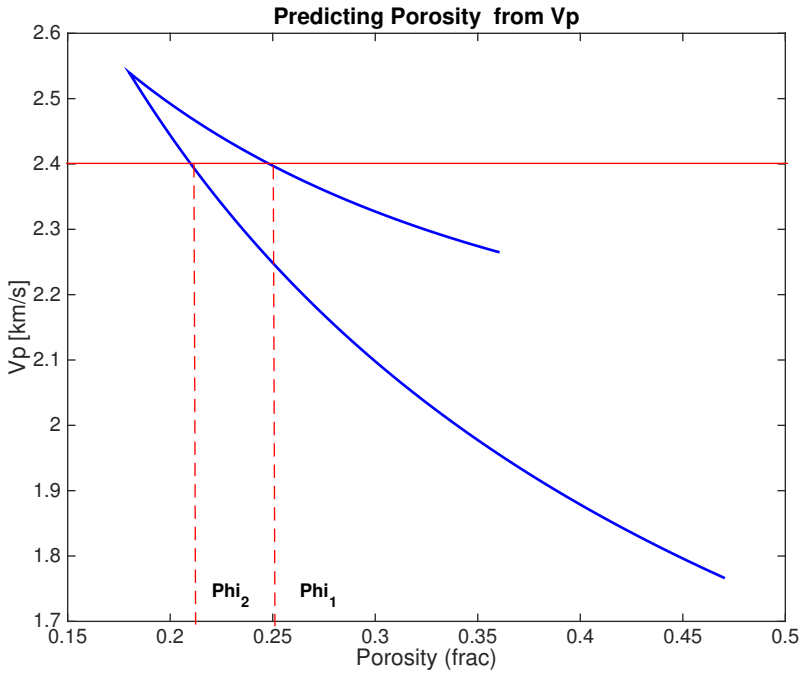

Figure 4.1: The figure shows Dvorkin modeled for a hypothetically case. To predict porosity from V_p, a specific velocity is inserted into the model, which will intersect the model in two points. These two points corresponds to two possible porosity points, ϕ_1 and ϕ_2. Note that the velocity will only intersect the model in one point for low velocities.

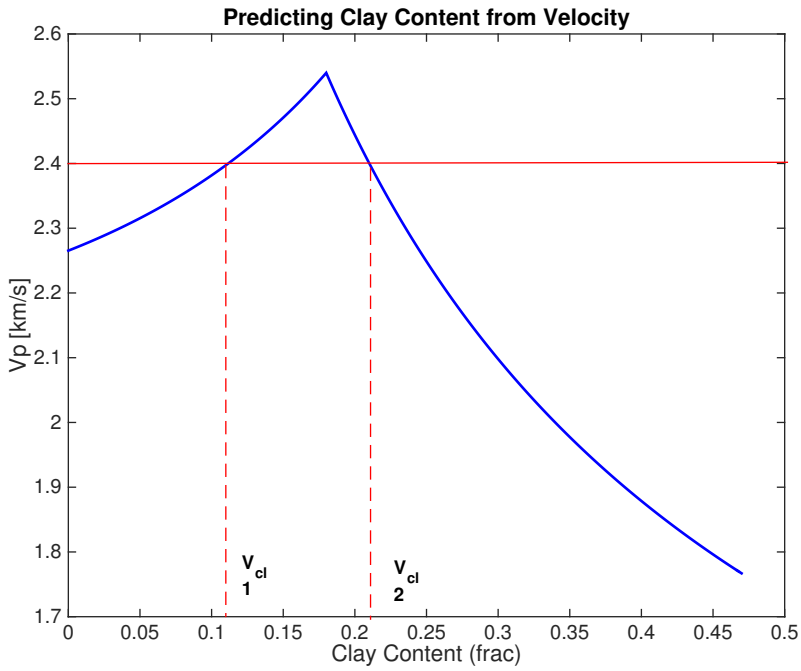

Figure 4.2: The figure shows Dvorkin modeled for a hypothetically case. To predict clay content from V_p, a specific velocity is inserted into the model, which will intersect the model in two points. These two points corresponds to two possible clay content points, $V_{cl}1$ and $V_{cl}2$. Note that the velocity will only intersect the model in one point for low velocities.

4.4.1 Calibrating for Overpressure

The velocity profile for all wells shows an interval where the velocity drops and follows a flat velocity trend. The low velocity zones are likely caused by the presence of smectite, and as presented in the Data Section, these zones are likely to be subject to overpressure.

To account for this effect, the two models are run for both a hydrostatic case and an overpressured case. The assumed overpressured zones are modeled by lowering the net stress, or w when using the modified BAM. The values used in the modeling can be found in the Appendix.

4.5 Values Used in the Modeling

The table below shows the values that have been used in the modeling of both the modified BAM and Dvorkin's Textural Sorting.

Constant	Unit	Value
K_{qtz}	GPa	38
G_{qtz}	GPa	44
M_{qtz}	GPa	96.67
K_f, K_b	GPa	2.2
K_{clay}	GPa	25
G_{clay}	GPa	8
C_{33Clay}	GPa	33.4
ρ_c	g/cm^3	2.35
ρ_s	g/cm^3	2.64
ρ_w	g/cm^3	1.03

Table 4.2: Constants and corresponding values that has been used in the modeling.

Chapter 5

Results

In this section the two models will be compared to both lab data presented in (Marion et al., 1992) and well data. Porosity and clay content have been predicted from compressional velocities, and the results are presented here.

5.1 The Modified BAM and Dvorkin Compared to Lab Data

The modified BAM and Dvorkin is compared to the lab data presented in Marion et al. (1992). The figures below show the relation between P-wave velocity, porosity, and clay content, and how the two models work compared to the results obtained from the lab experiment.

σ'	w
9 MPa	0.07
19 MPa	0.08
29 MPa	0.1
39 MPa	0.11
49 MPa	0.12

Table 5.1: Values for w at corresponding net stresses.

5.1.1 Porosity as a Function of Clay Content

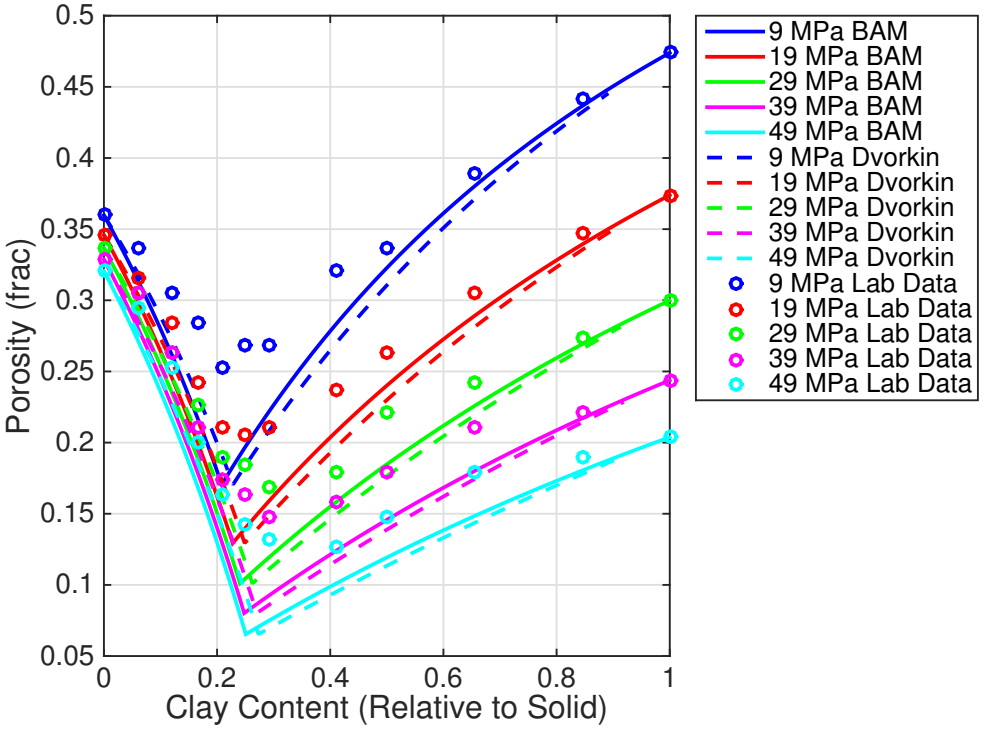

Figure 5.1: Porosity as a function of clay content for various net stresses. The scattered points are the data obtained from lab experiment (Data courtesy: Marion et al. (1992)). The two models give results that are quite similar, but the Dvorkin-model is slightly shifted to the right compared to the modified BAM-model. In addition, the Dvorkin-model has a maximum clay content of about 0.9, while the modified BAM-model has its maximum at 1. Compared to the lab data, the two models give accurate results for very low clay contents (sand) and very high clay contents (shale). However, the results deviate as the models transitions from shaley sand to sandy shale, yielding lower porosities than that obtained from the lab data. The porosity minimum is also shifted to the left for the two models compared to the lab data.

5.1.2 P-Wave Velocity as a Function of Porosity

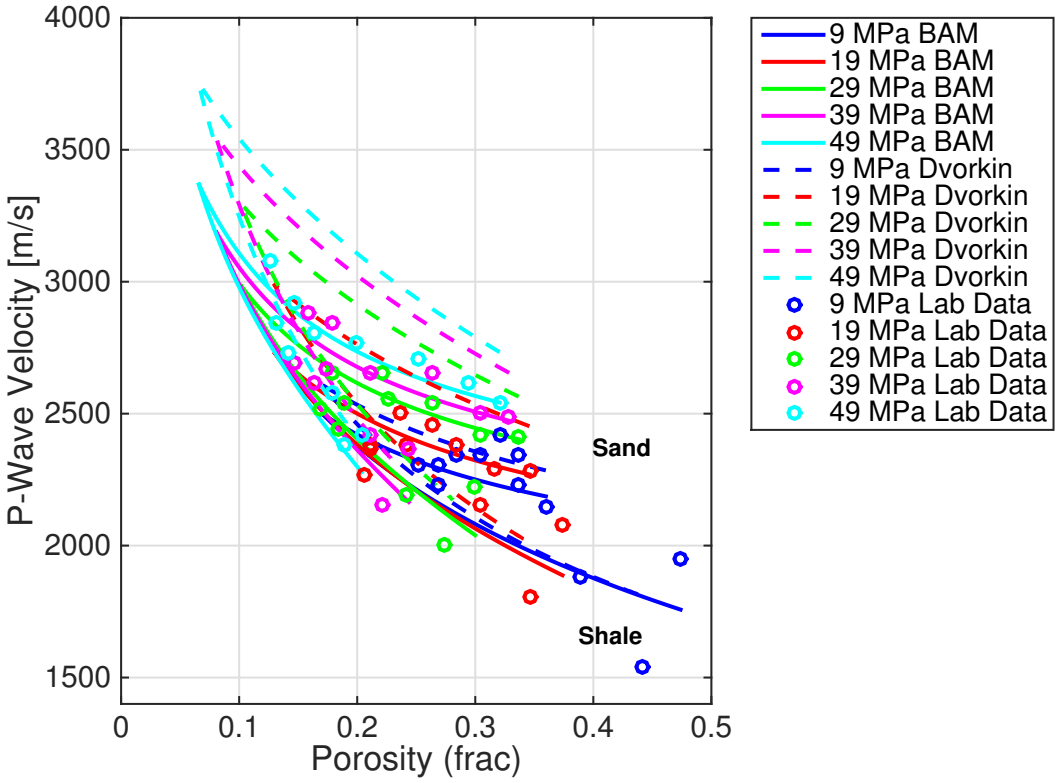

Figure 5.2: P-wave velocity as a function of porosity for various net stresses. The scattered points are the data obtained from lab experiment (Data courtesy: Marion et al. (1992)). Using Dvorkin yields a stiffer result than the results obtained using the modified BAM, causing higher velocities which deviate from the lab data.

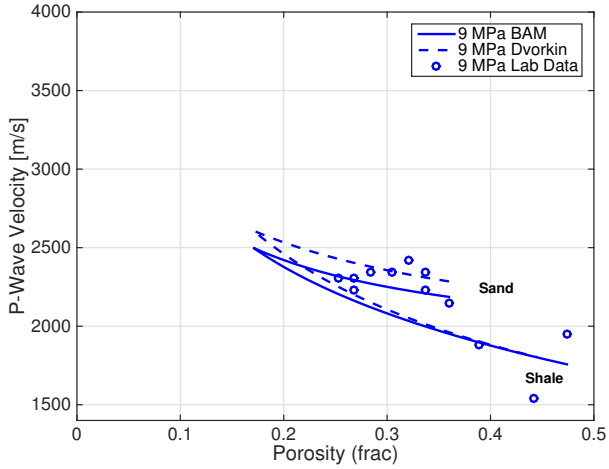

((a)) P-wave velocity vs. porosity for the modified BAM and Dvorkin at a net stress of 9 MPA

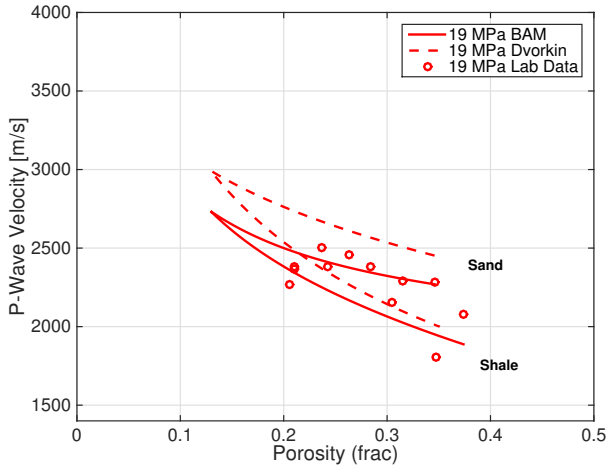

((b)) P-wave velocity vs.porosity for the modified BAM and Dvorkin at a net stress of 19 MPA

Figure 5.3: Porosity as a function of P-wave velocity at a differential pressure of 9 MPa and 19 MPa. The scattered points are the data obtained from lab experiment (Data courtesy: (Marion et al., 1992)). Using Dvorkin results in higher velocities. The lab data are more aligned with the modified BAM model.

5.1.3 P-Wave Velocity as a Function of Clay Content

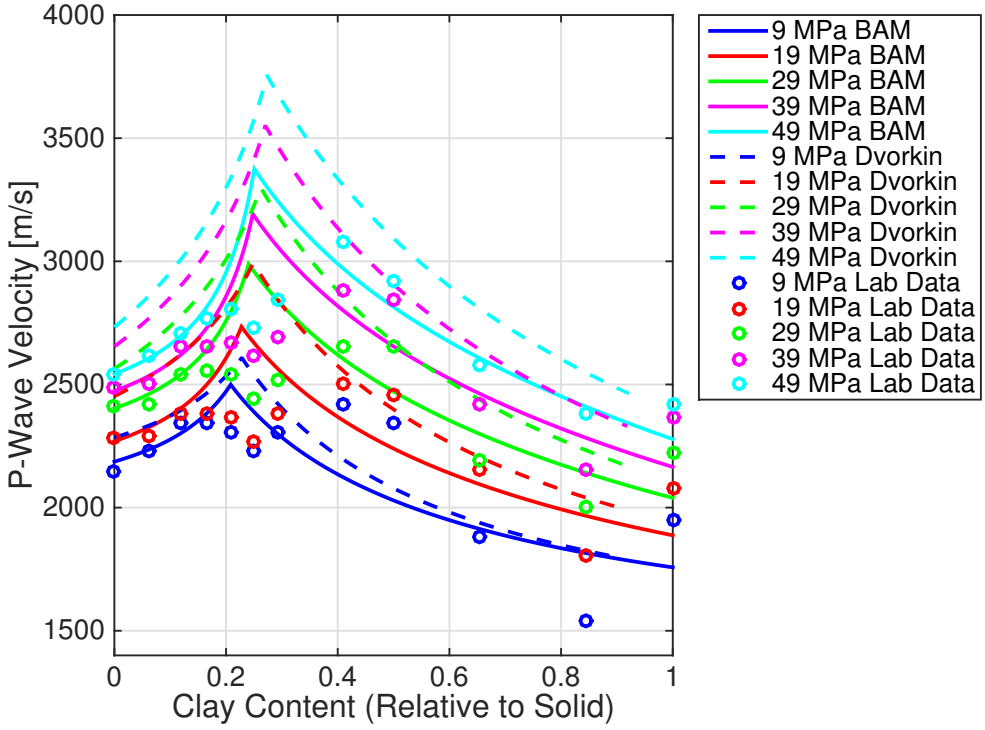

Figure 5.4: P-wave velocity as a function of clay content for various differential pressures. The scattered points are the data obtained from lab experiment (Data courtesy: Marion et al. (1992)). Again, it becomes evident that Dvorkin yields higher velocities than the modified BAM. Also here, the lab data are more aligned with the BAM-model than Dvorkin.

5.2 The Modified BAM and Dvorkin Compared to Well 6608/10-3

5.2.1 Calibrating the Models to the Well

The calibration of the models to the well have been carried out as explained in Chapter 4. The values used in the calibration are listed in Table 5.2.

σ'	ϕ_s	ϕ_{sh}	w
9 MPa	0.36	0.45	0.11
19 MPa	0.36	0.55	0.14
27 MPa	0.32	0.25	0.3

Table 5.2: Calibrated values for ϕ_s and ϕ_{sh} at the corresponding net stresses. Note the low value of w needed to fit the model to the well data at a net stress of 19 MPa.

Calibration at 9 MPa

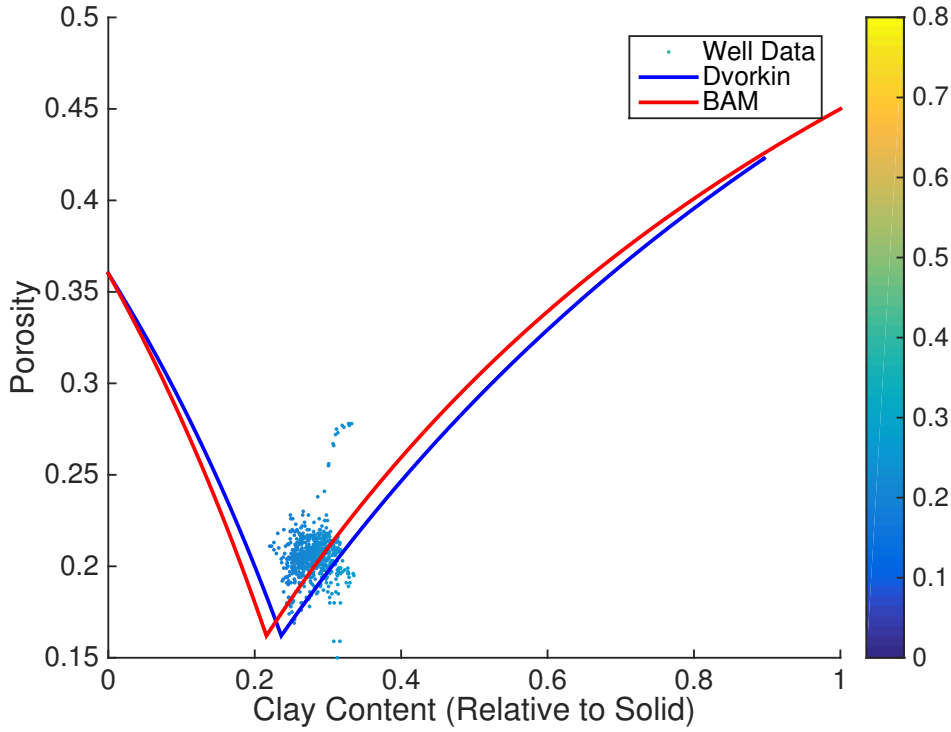

Figure 5.5: Porosity vs. clay content for the modified BAM, Dvorkin, and the well data at a net stress of 9 MPa. The two models are calibrated in such a way that they intersect the well data points.

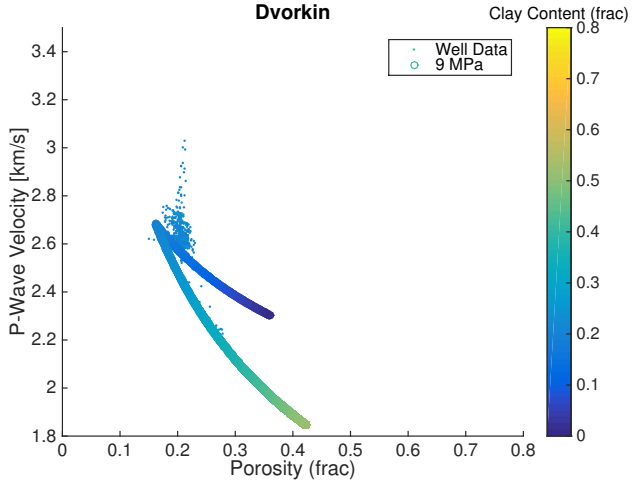

((a)) P-wave velocity vs. porosity at a net stress of 9 MPa using Dvorkin. Color coding corresponds to the clay content both in the model and the well data. The model aligns well with the well data.

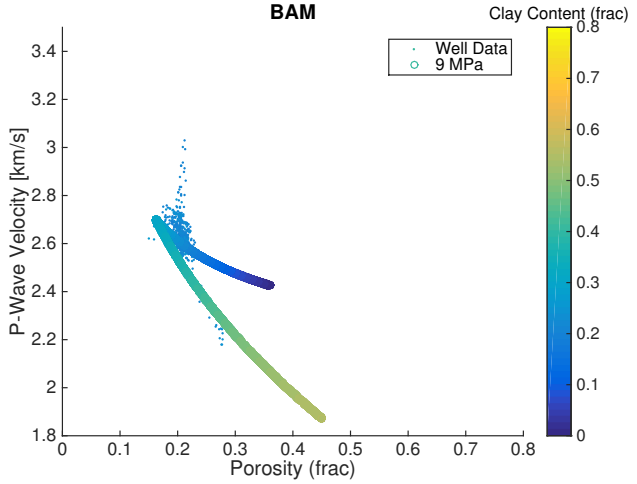

((b)) P-wave velocity vs. porosity at a net stress of 9 MPa using the modified BAM. Color coding corresponds to the clay content both in the model and the well data. The model aligns well with the well data.

Figure 5.6: Velocity, porosity, and clay content for the modified BAM, Dvorkin, and the well data at a net stress of 9 MPa.

Calibration at 19 MPa

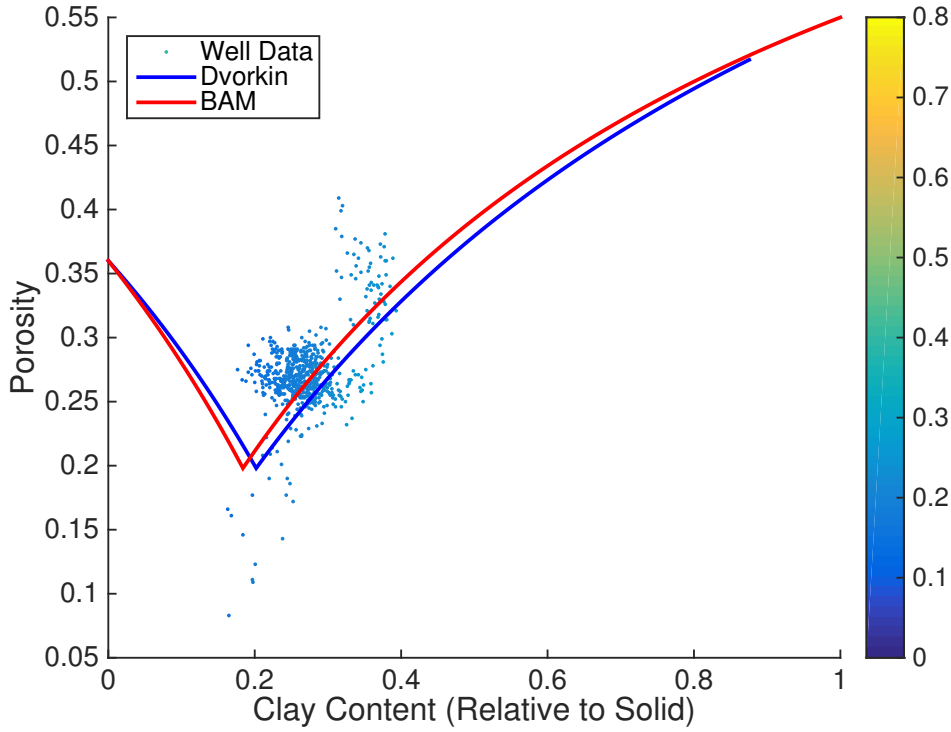

Figure 5.7: Porosity vs. clay content for the modified BAM, Dvorkin, and the well data at a net stress of 19 MPa. The two models are calibrated in such a way that they intersect the well data points.

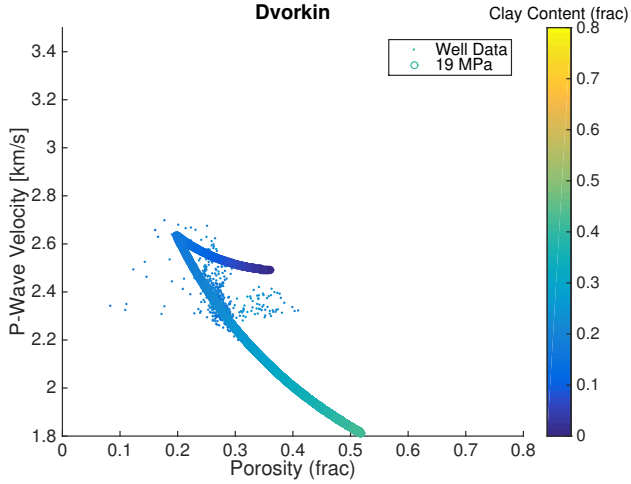

((a)) P-wave velocity vs. porosity at a net stress of 19 MPa using Dvorkin. Color coding corresponds to the clay content both in the model and the well data. The model aligns well with the well data.

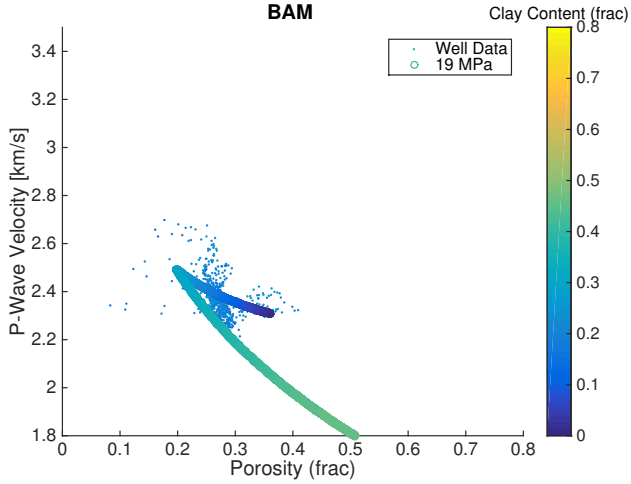

((b)) P-wave velocity vs. porosity at a net stress of 19 MPa using the modified BAM. Color coding corresponds to the clay content both in the model and the well data. The model aligns well with the well data.

Figure 5.8: Velocity, porosity, and clay content for the modified BAM, Dvorkin, and the well data at a net stress of 19 MPa.

Calibration at 27 MPa

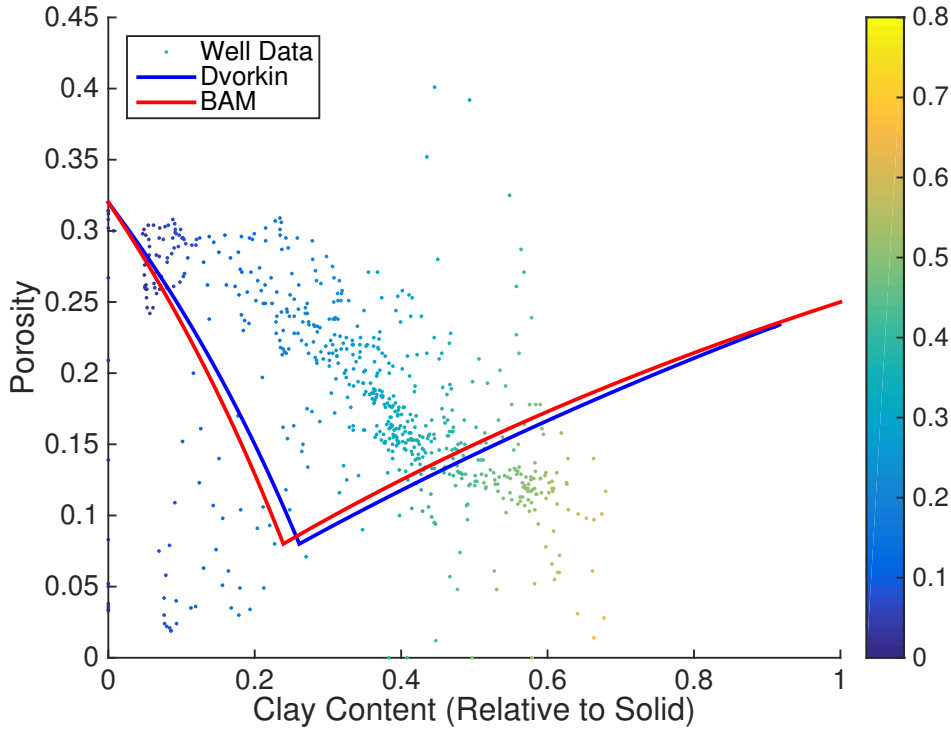

Figure 5.9: Porosity vs. clay content for the modified BAM, Dvorkin, and the well data at a net stress of 27 MPa. The two models are calibrated in such a way that they intersect the well data points.

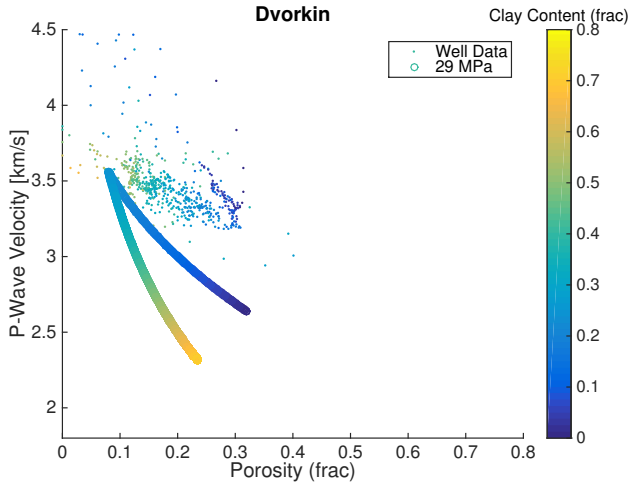

((a)) P-wave velocity vs. porosity at a net stress of 27 MPa using the Dvorkin. Color coding corresponds to the clay content both in the model and the well data. The model fails to capture the porosity - clay content trend.

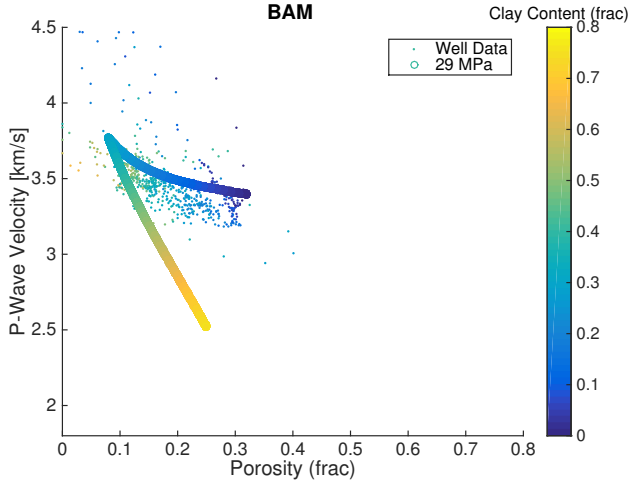

((b)) P-wave velocity vs. porosity at a net stress of 27 MPa using the modified BAM. Color coding corresponds to the clay content both in the model and the well data. The model aligns well with the well data.

Figure 5.10: Velocity, porosity, and clay content for the modified BAM, Dvorkin, and the well data at a net stress of 27 MPa.

5.2.2 Predicting Porosity and Clay Content from Velocity

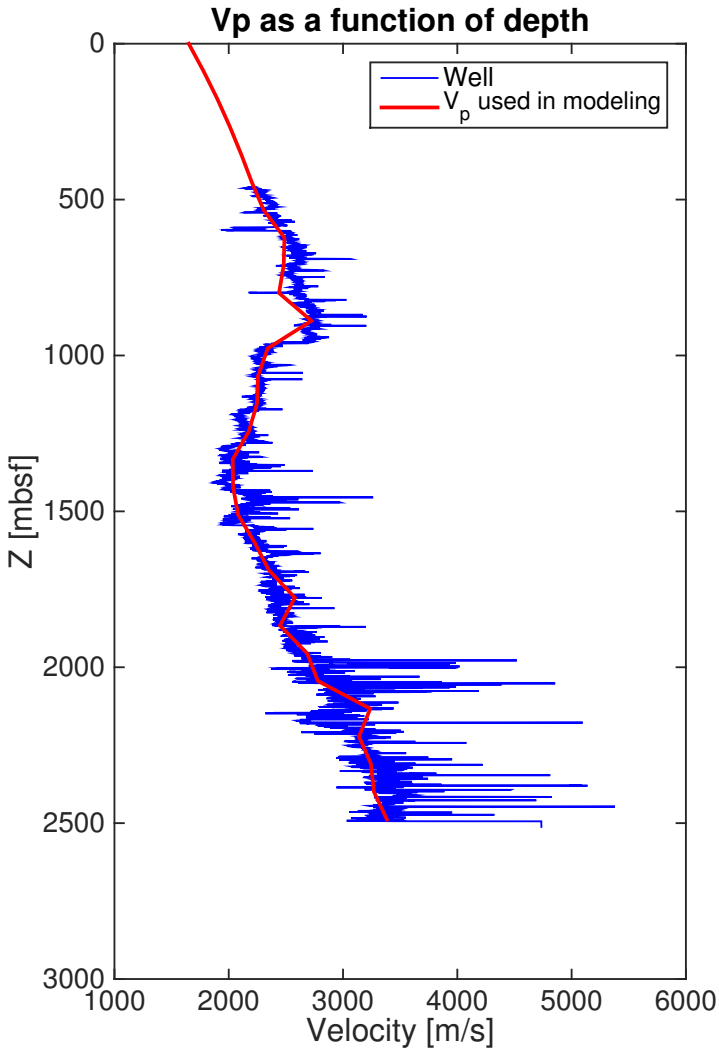

Figure 5.11: Well 6608/10-3: The figure shows the compressional velocity obtained from the well log (blue line). The red line represents the velocities used as an input parameter when estimating porosity and clay content from the two models.

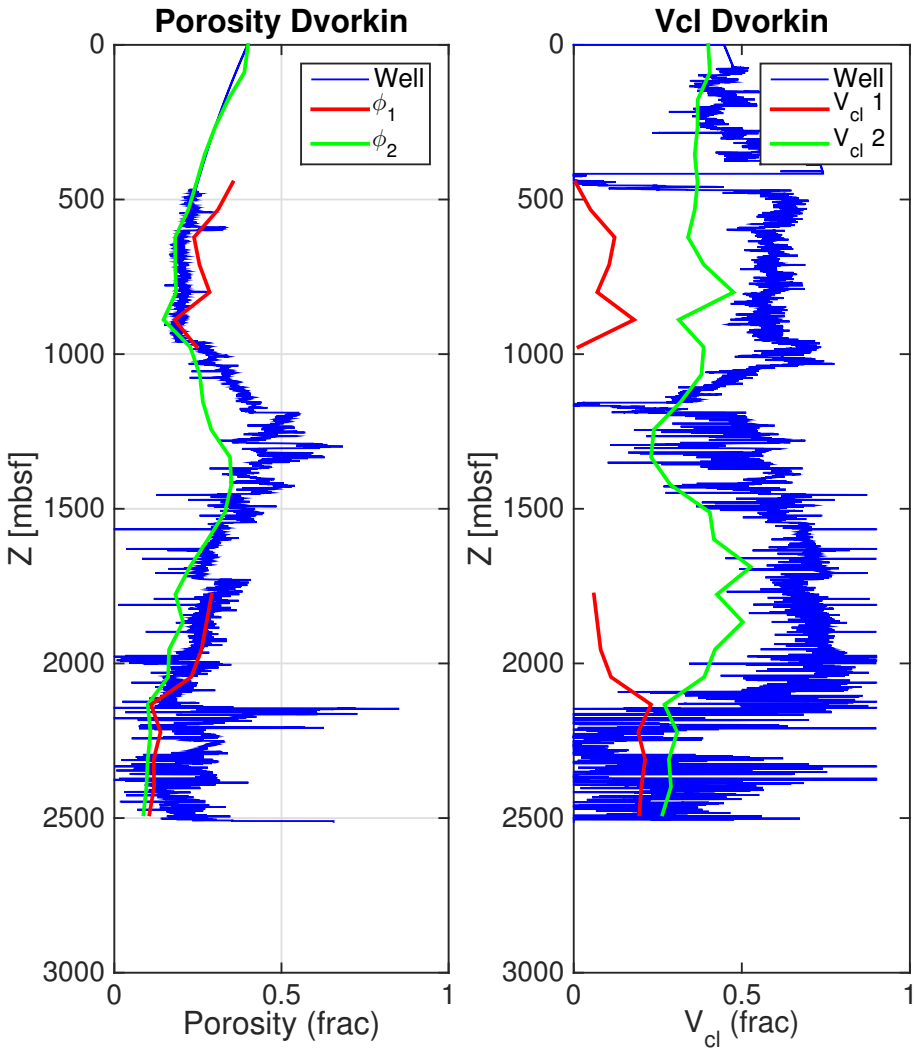

Figure 5.12: Well 6608/10-3: The figure shows the estimated porosity (left) and clay content (right) plotted with the well data. The red and green lines represent the estimated porosity and clay content values from using the Dvorkin model. At each step, the predicted porosity and clay content corresponds to either the two red lines/points or the two green lines/points. The estimated porosity is overall good, but is underpredicted in the assumed overpressured zone, corresponding to a depth of approximately 1000-1500 mbsf. The clay content gives a less accurate estimation compared to the porosity estimation, where the clay content is in general underpredicted. The most accurate estimations are obtained by the green line (ϕ_2 and $V_{cl}2$).

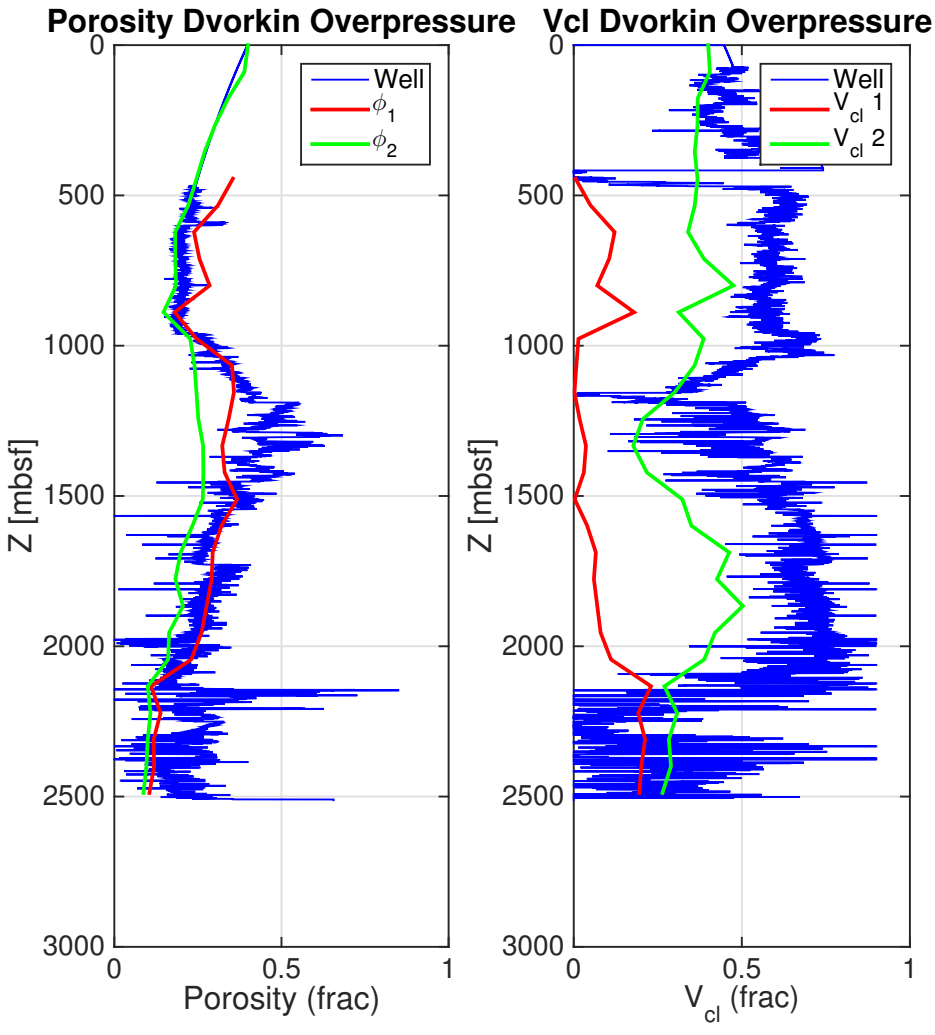

Figure 5.13: Well 6608/10-3: The figure shows the estimated porosity (left) and clay content (right) plotted with the well data. The red and green lines represent the estimated porosity and clay content values from using the Dvorkin model when assuming overpressure in the interval corresponding to 1000-1500 mbsf. At each step, the predicted porosity and clay content corresponds to either the two red lines/points or the two green lines/points. The estimated porosity is overall good, but is highly underpredicted in the assumed overpressured zone. The clay content gives a less accurate estimation compared to the porosity estimation, where the clay content is in general underpredicted. The most accurate estimations are obtained by the green line (ϕ_2 and $V_{cl}2$).

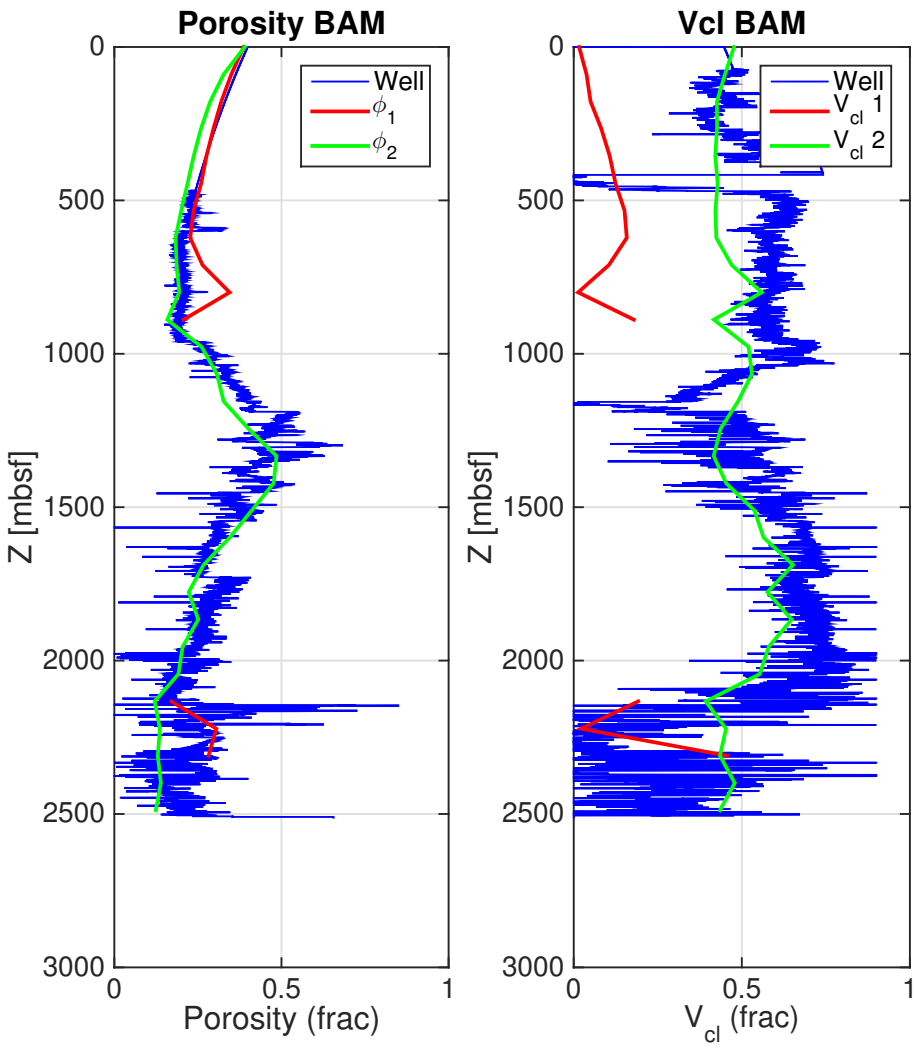

Figure 5.14: Well 6608/10-3: The figure shows the estimated porosity (left) and clay content (right) plotted with the well data. The red and green lines represent the estimated porosity and clay content values from using the Modified BAM model. At each step, the predicted porosity and clay content corresponds to either the two red lines/points or the two green lines/points. The predicted porosity is a good match to the porosity obtained from the well log. The clay content is in general underpredicted in most intervals, but seems to follow the trend of the clay content obtained from the well log. The most accurate estimations are obtained by the green line (ϕ_2 and $V_{cl}2$).

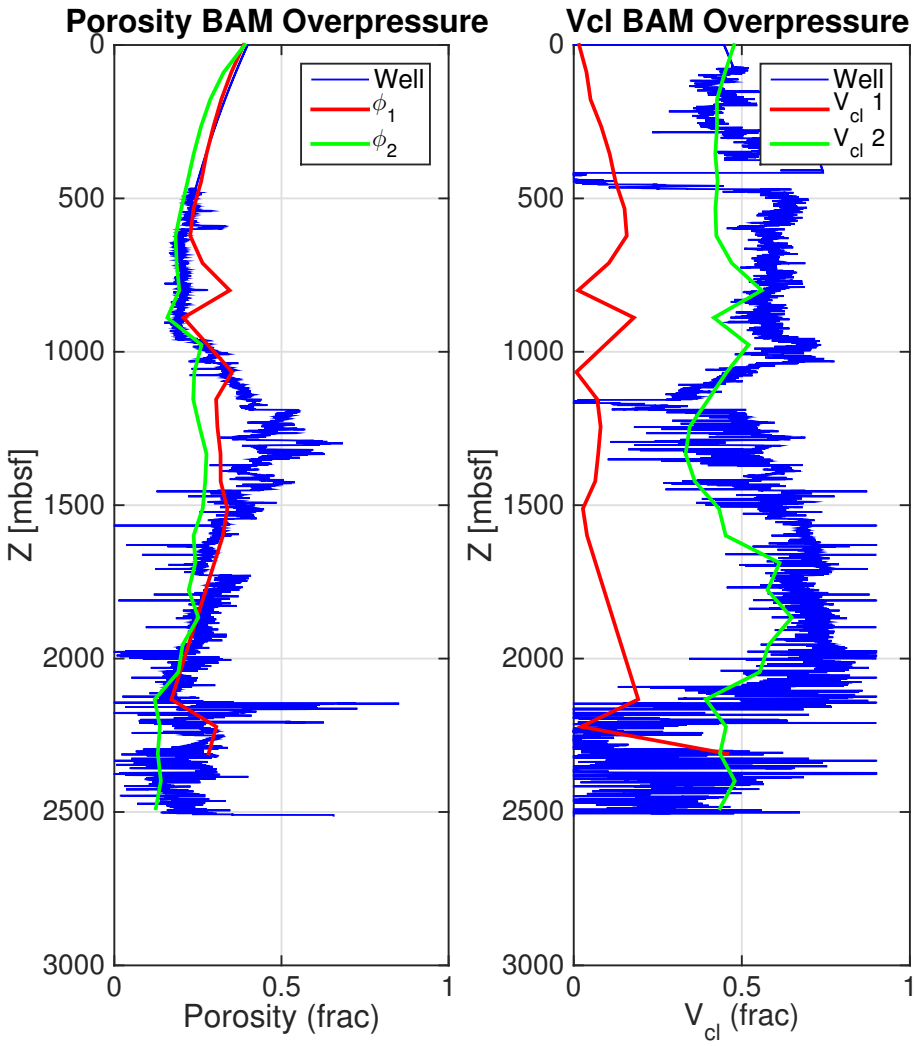

Figure 5.15: Well 6608/10-3: The figure shows the estimated porosity (left) and clay content (right) plotted with the well data. The red and green lines represent the estimated porosity and clay content values from using the Modified BAM model. At each step, the predicted porosity and clay content corresponds to either the two red lines/points or the two green lines/points. The predicted porosity is a good match to the porosity obtained from the well log, but is underpredicted in the assumed overpressured zone, corresponding to a depth of approximately 1000-1500 mbsf. The clay content is in general underpredicted in most intervals, but seems to follow the trend of the clay content obtained from the well log. The most accurate estimations are obtained by the green line (ϕ_2 and $V_{cl}2$).

5.3 The Modfied BAM and Dvorkin Compared to Well 34/7-1

5.3.1 Predicting Porosity and Clay Content from Velocity

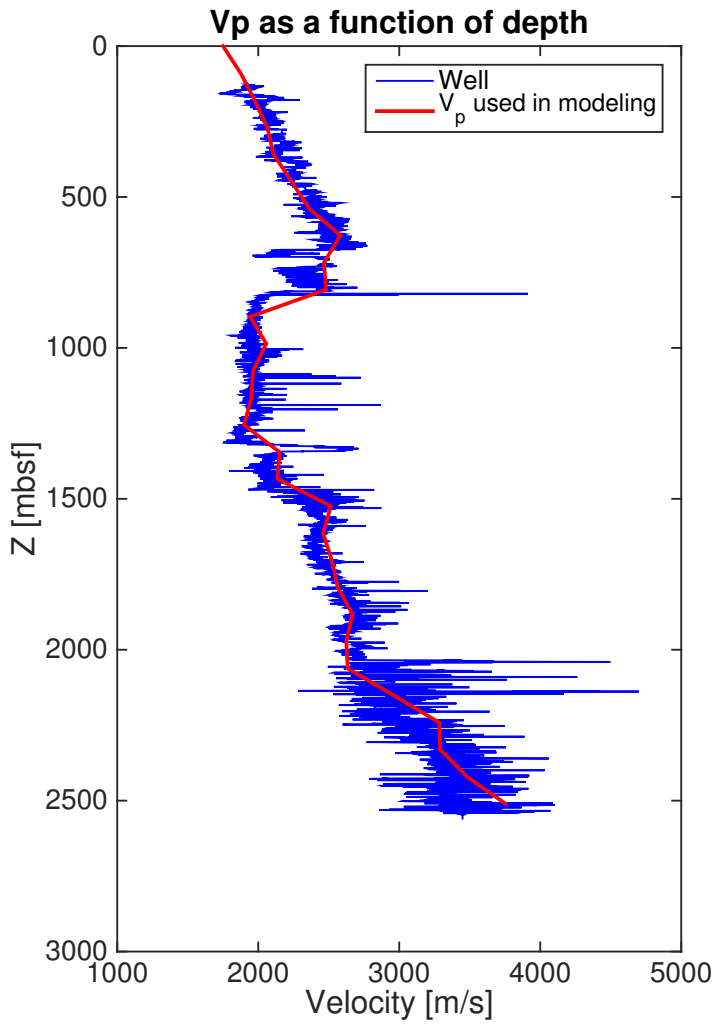

Figure 5.16: Well 34/7-1: The figure shows the compressional velocity obtained from the well log (blue line). The red line represents the velocities used as an input parameter when estimating porosity and clay content from the two models.

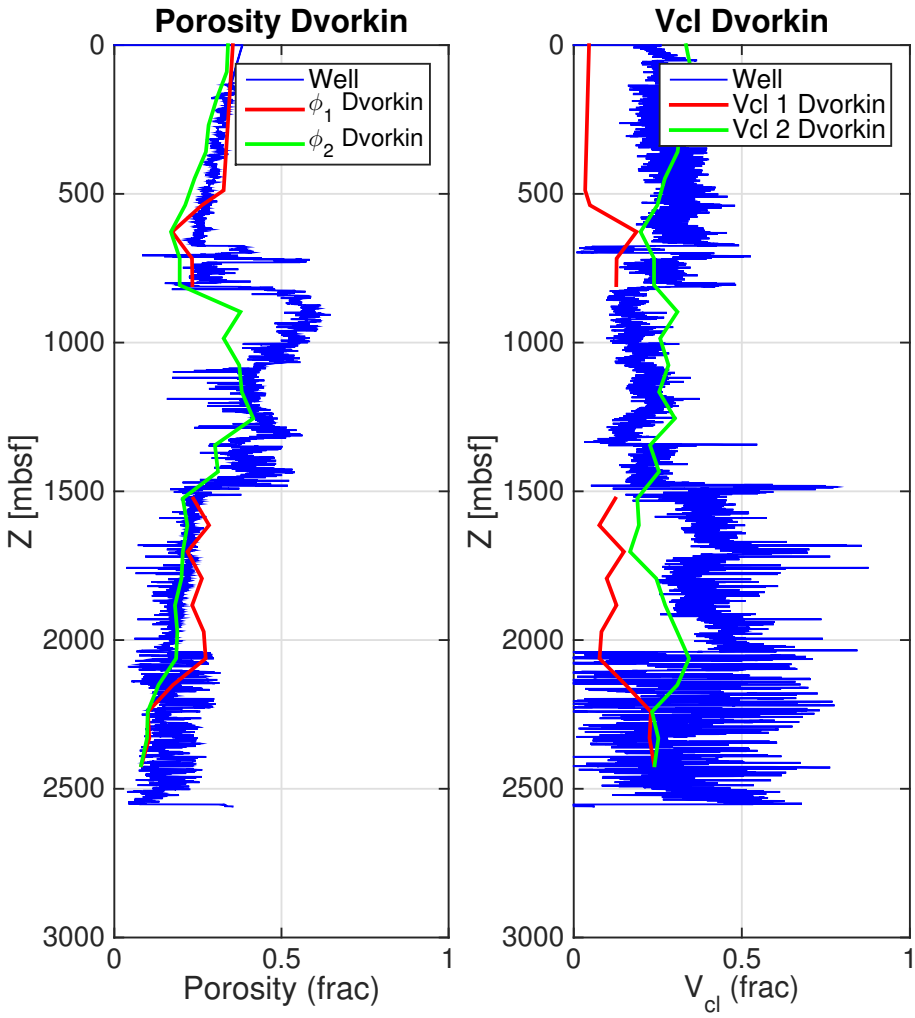

Figure 5.17: Well 34/7-1: The figure shows the estimated porosity (left) and clay content (right) plotted with the well data. The red and green lines represent the estimated porosity and clay content values from using the Dvorkin model. At each step, the predicted porosity and clay content corresponds to either the two red lines/points or the two green lines/points. The predicted porosity is a good match to the porosity obtained from the well log, but seems to underpredict in the assumed overpressured zone, corresponding to a depth of 800-1500 mbsf. The clay content is somewhat overpredicted in the assumed overpressued zone, while it is underpredicted in the interval 1500-2000 mbsf. Overall, the estimated clay content captures the trend of the clay content obtained from the well log. The most accurate estimations are obtained by the green line (ϕ_2 and $V_{cl}2$).

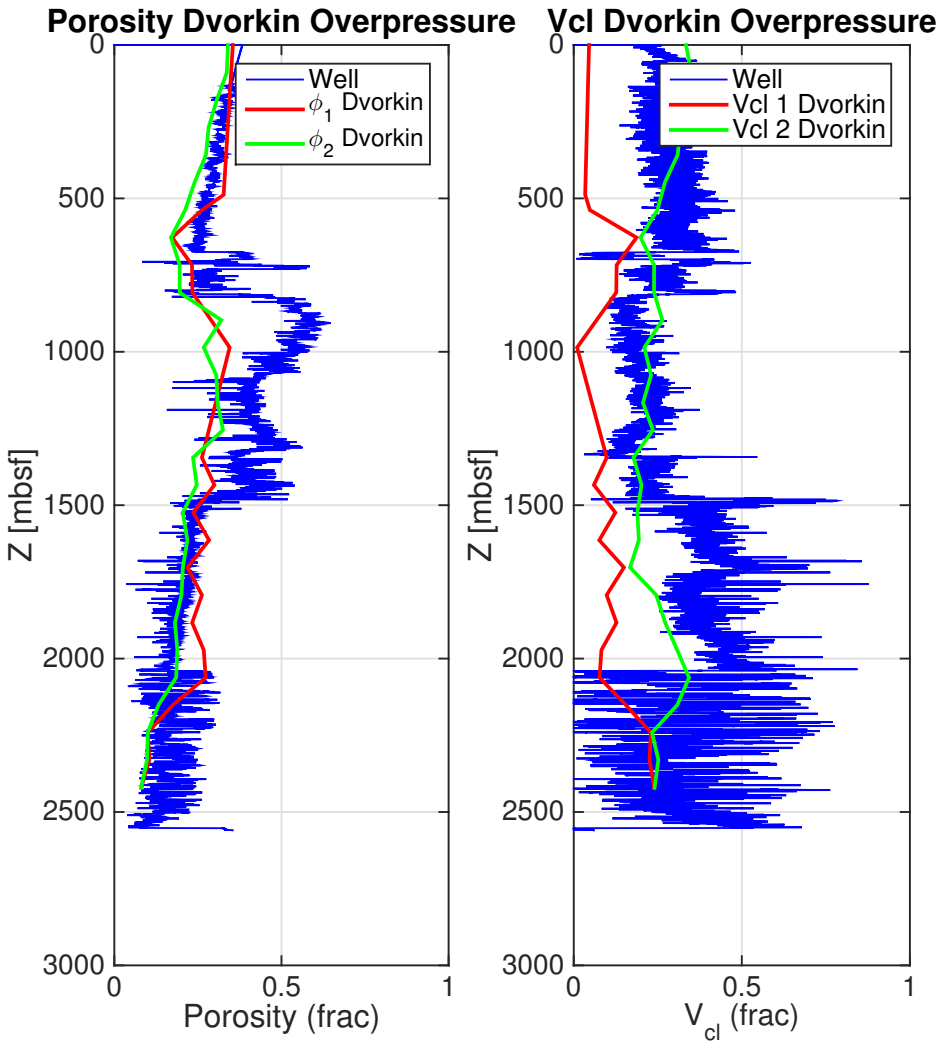

Figure 5.18: Well 34/7-1: The figure shows the estimated porosity (left) and clay content (right) plotted with the well data. The red and green lines represent the estimated porosity and clay content values from using the Dvorkin model when assuming overpressure in the interval corresponding to a depth of 800-1500 mbsf. At each step, the predicted porosity and clay content corresponds to either the two red lines/points or the two green lines/points. The predicted porosity gives an overall good match to the porosity obtained from the well log, but is underpredicted in the assumed overpressured zone. The clay content is underpredicted in the interval corresponding to a depth of 1500-2000 mbsf, but captures the general trend of the clay content obtained from the well log. The most accurate estimations are obtained by the green line (ϕ_2 and $V_{cl}2$)..

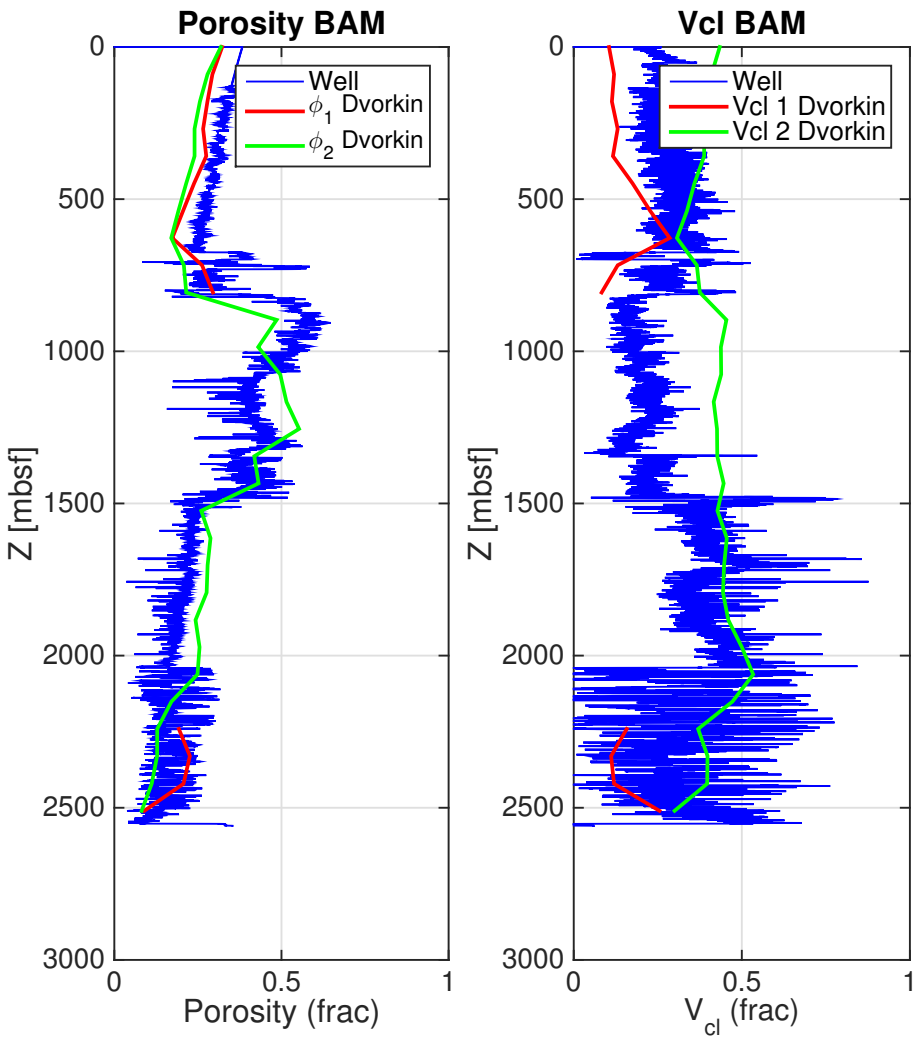

Figure 5.19: Well 34/7-1: The figure shows the estimated porosity (left) and clay content (right) plotted with the well data. The red and green lines represent the estimated porosity and clay content values from using the modified BAM model. At each step, the predicted porosity and clay content corresponds to either the two red lines/points or the two green lines/points. The predicted porosity is a good match to the porosity obtained from the well log, showing only small deviations from the well log. The clay content seems to be highly overpredicted in the assumed overpressued zone, corresponding to a depth of 800-1500 mbsf. Overall, the estimated clay content captures the trend of the well log. Both the red and blue lines seems like reasonable estimations.

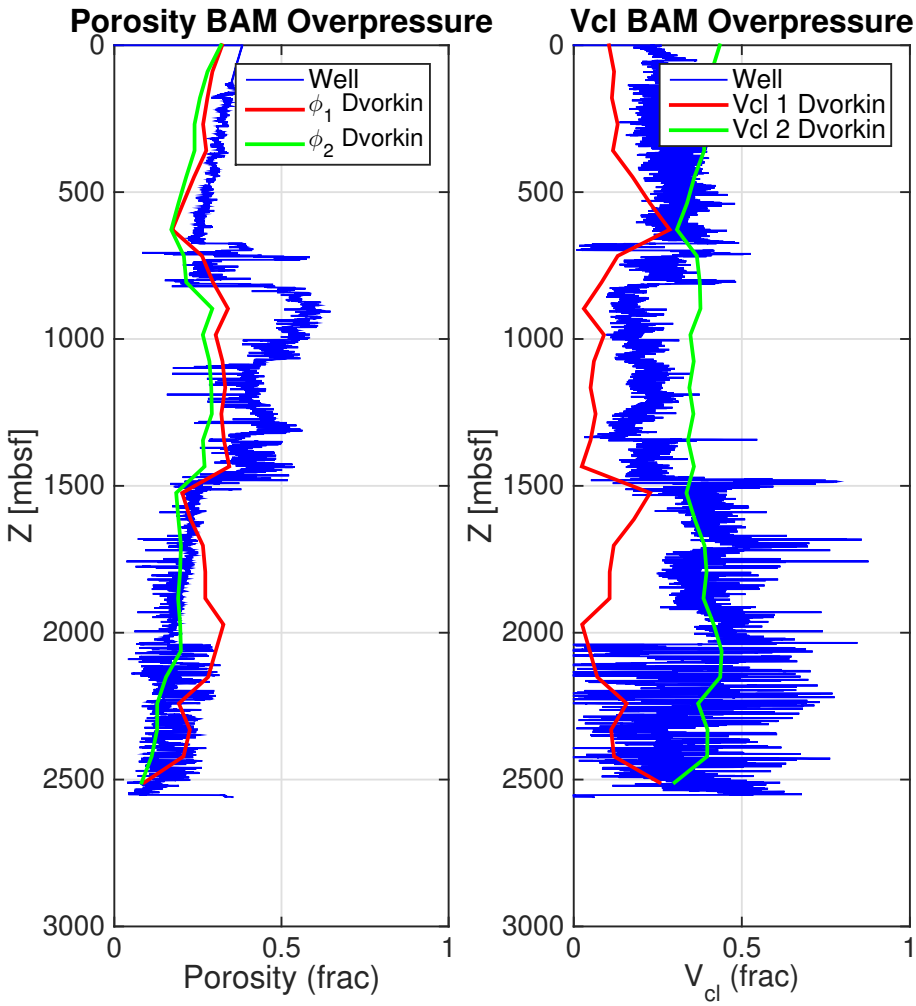

Figure 5.20: Well 34/7-1: The figure shows the estimated porosity (left) and clay content (right) plotted with the well data. The red and green lines represent the estimated porosity and clay content values from using the the modfied BAM model when assuming overpressure in the interval corresponding to a depth of 800-1500 mbsf. At each step, the predicted porosity and clay content corresponds to either the two red lines/points or the two green lines/points. The predicted porosity is a good match to the porosity obtained from the well log, but is highly underpredicted in the assumed overpressured zone. In the same interval, the clay content is overpredicted for the green line, while it is underpredicted for the red line. Overall, the estimated clay content captures the trend of the well log. The most accurate estimations are obtained by the green line (ϕ_2 and $V_{cl}2$).

5.4 The Modfied BAM and Dvorkin Compared to Well 33/5-2

5.4.1 Predicting Porosity and Clay Content from Velocity

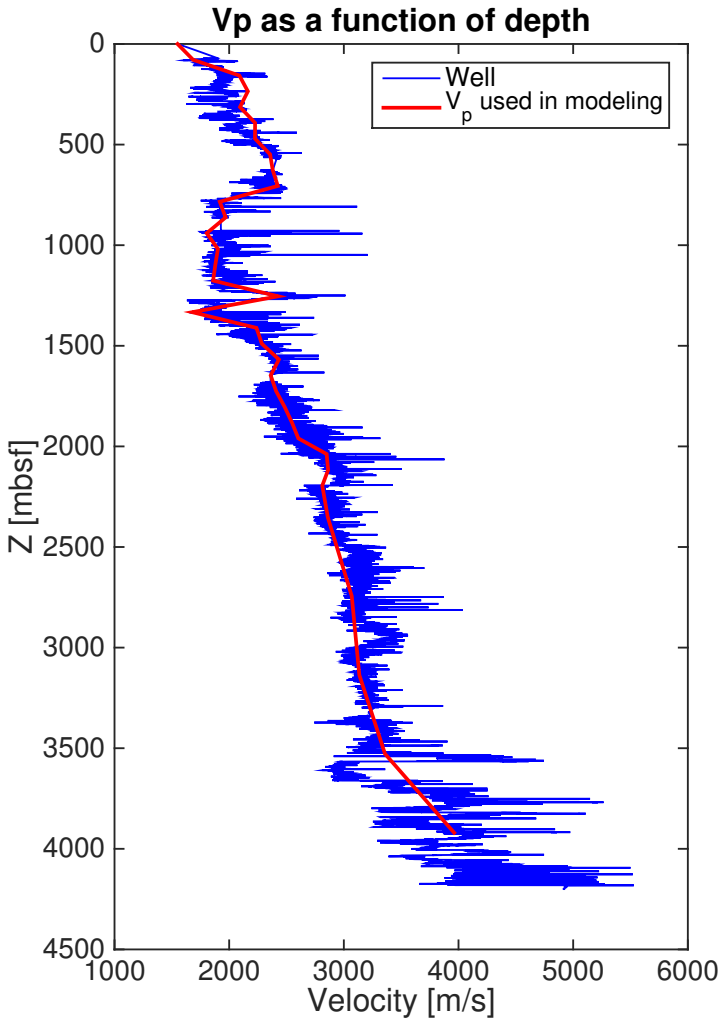

Figure 5.21: Well 33/5-2: The figure shows the compressional velocity obtained from the well log (blue line). The red line represents the velocities used as an input parameter when estimating porosity and clay content from the two models.

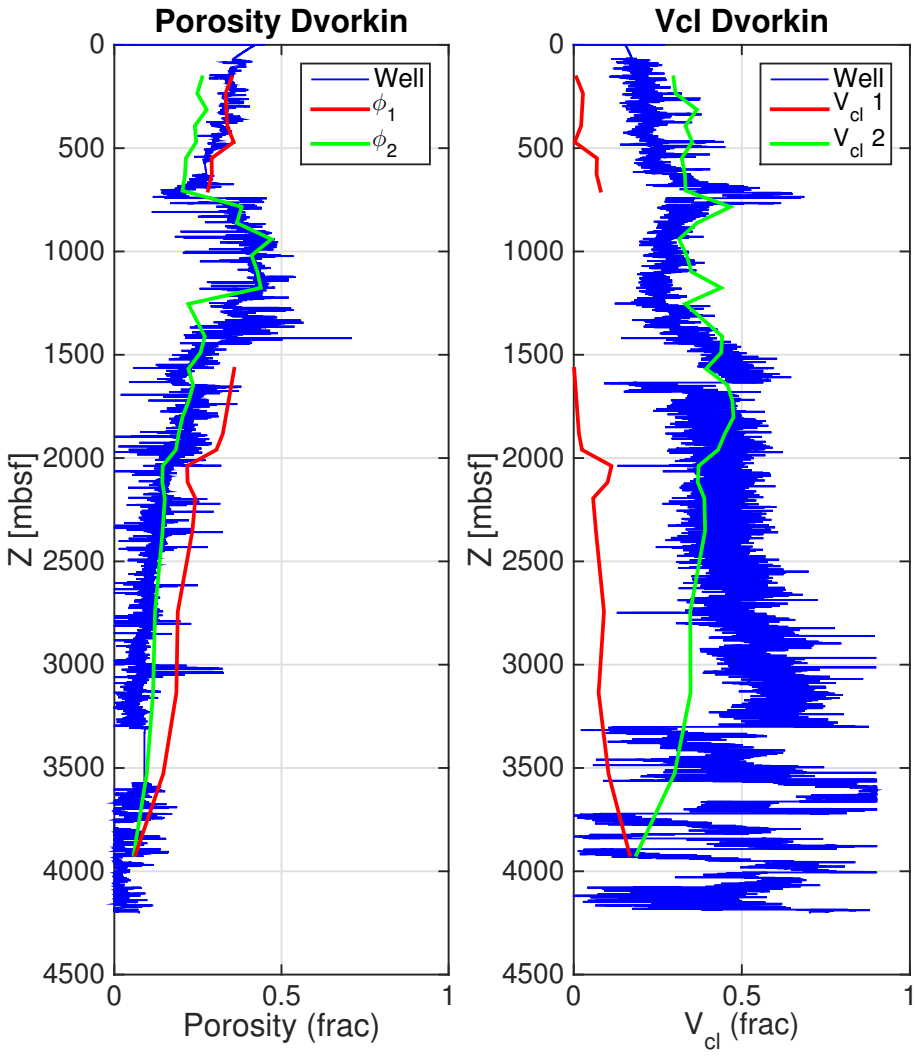

Figure 5.22: Well 33/5-2: The figure shows the estimated porosity (left) and clay content (right) plotted with the well data. The red and green lines represent the estimated porosity and clay content values from using the Dvorkin model. At each step, the predicted porosity and clay content corresponds to either the two red lines/points or the two green lines/points. The predicted porosity is a good match to the porosity obtained from the well log, only showing small deviations. The porosity is slightly overpredicted at great depths, where also the clay content is underpredicted (corresponding to a depth of 2200-4000 mbsf). Overall, the estimated clay content captures the trend of the well log. The most accurate estimations are obtained by the green line (ϕ_2 and $V_{cl}2$).

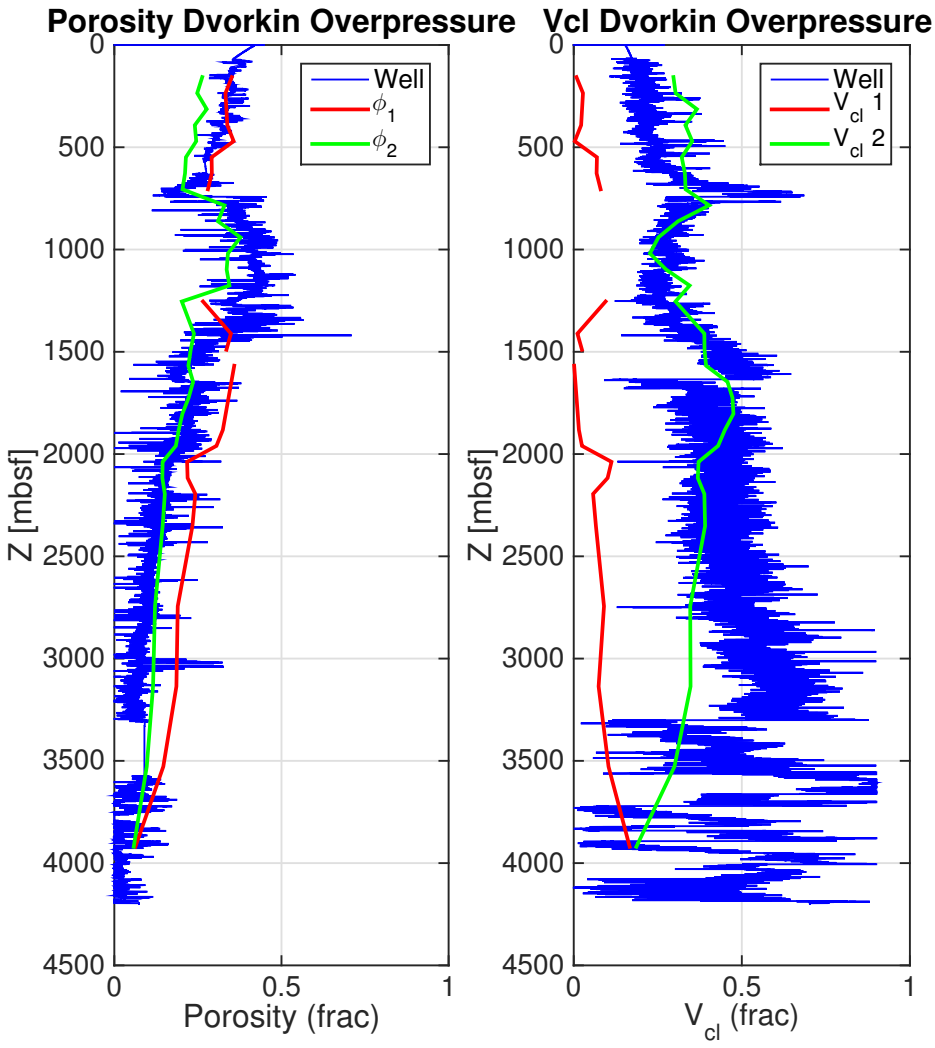

Figure 5.23: Well 33/5-2: The figure shows the estimated porosity (left) and clay content (right) plotted with the well data. The red and green lines represent the estimated porosity and clay content values from using the Dvorkin model when assuming overpressure in the interval corresponding to a depth of 800-1500 mbsf. At each step, the predicted porosity and clay content corresponds to either the two red lines/points or the two green lines/points. The predicted porosity is a good match to the porosity obtained from the well log, but is slightly underpredicted in the assumed overpressured zone. The clay content in the same zone matches the well log in a better way than when not assuming overpressure. Overall, the estimated clay content captures the trend of the clay content obtained from the well log. The most accurate estimations are obtained by the green line (ϕ_2 and $V_{cl}2$).

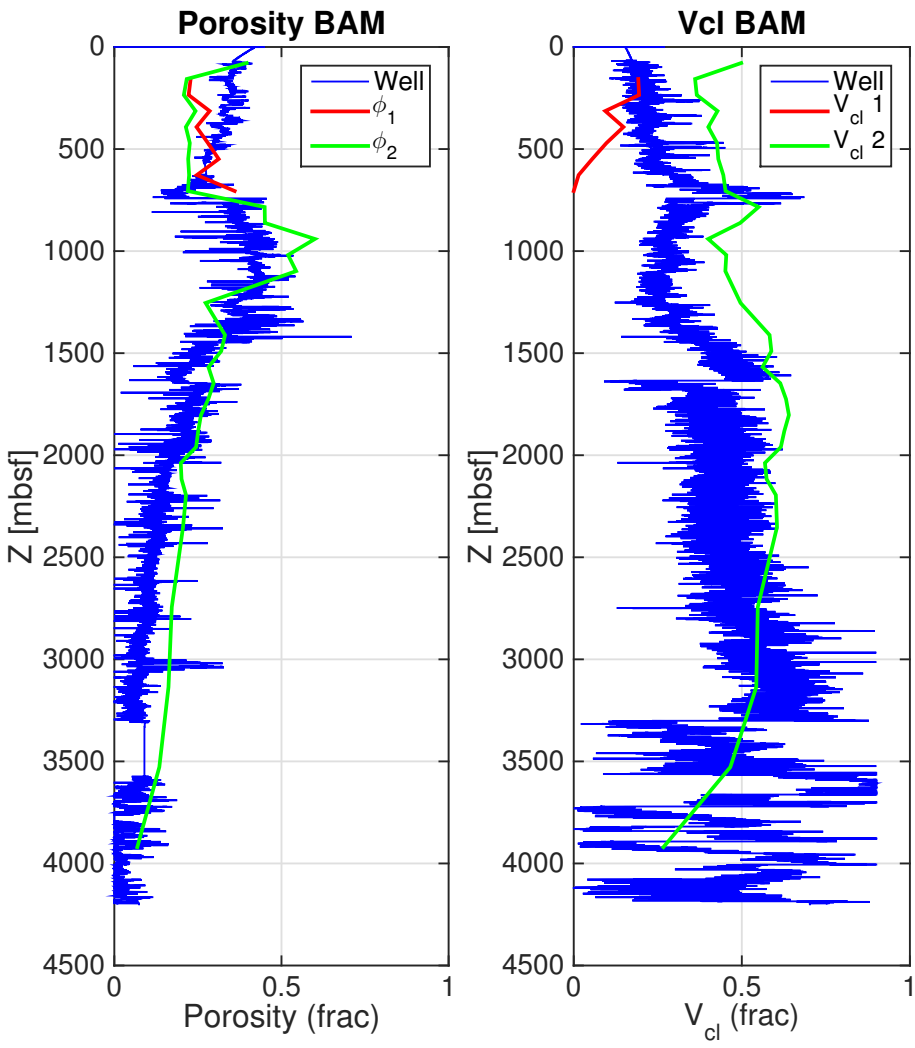

Figure 5.24: Well 33/5-2: The figure shows the estimated porosity (left) and clay content (right) plotted with the well data. The red and green lines represent the estimated porosity and clay content values from using the modified BAM model. At each step, the predicted porosity and clay content corresponds to either the two red lines/points or the two green lines/points. The predicted porosity offers an overall good match with the well log, but is slightly overpredicted in the assumed overpressued zone, corresponding to a depth of 800-1500 mbsf. Also, the porosity is slightly overpredicted in the deeper parts of the well, corresponding to a depth of 2000-3500 mbsf. The estimated clay content seems to capture the trend, but is somewhat overpredicted, especially in the assumed overpressured zone. The most accurate estimations are obtained by the green line (ϕ_2 and $V_{cl}2$).

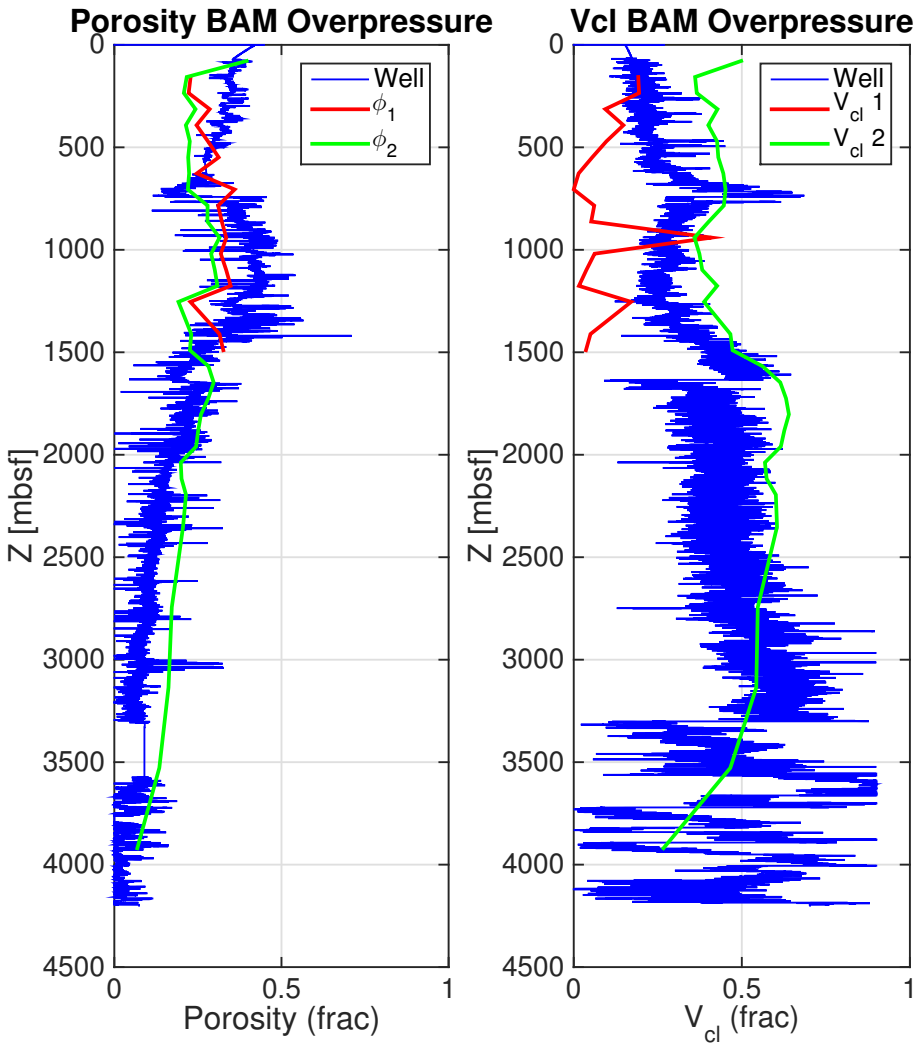

Figure 5.25: Well 33/5-2: The figure shows the estimated porosity (left) and clay content (right) plotted with the well data. The red and green lines represent the estimated porosity and clay content values from using the modified BAM model when assuming overpressure in the interval corresponding to a depth of 800-1500 mbsf. At each step, the predicted porosity and clay content corresponds to either the two red lines/points or the two green lines/points. The predicted porosity is a good match to the porosity obtained from the well log, but is slightly underpredicted in the assumed overpressured zone, and also slightly overpredicted in the deeper parts of the well, corresponding to a depth of 2000-3500 mbsf. The clay content in the assumed overpressured zone matches the well log in a better way than when not assuming overpressure. The general clay content trend is captured by the estimations, but does tend to be overpredicted. The most accurate estimations are obtained by the green line (ϕ_2 and $V_{cl}2$).

Chapter 6

Discussion

In the previous sections it has been shown how porosity can be calculated for a binary system consisting of sand and clay, and how the relation between porosity, clay content, and velocity can be used for predictive purposes. The two models, the modified BAM and Dvorkin, have been tested on both lab data and well data from the Norwegian Continental Shelf, and in the following section the findings will be discussed.

6.1 The Modified BAM and Dvorkin Compared to Lab Data

Figure 5.1 shows porosity as a function of clay content for both the modified BAM and Dvorkin compared to lab data. It is evident that the two models yield almost identical porosity models, where Dvorkin only gives a slightly lower estimate of the porosity compared to the modified BAM (also note that the Dvorkin model has a maximum clay content of 0.9, whereas the modified BAM has a maximum of 1.0). However, the two models underestimate the porosity in the shaley sand and sandy shale domain, where only the end points (clean sand and clean shale) are estimated accurately. The greatest difference is seen in the minimum porosity point, where the two models estimate the porosity to be 48 % (at 9 MPa) to 93 % (49 MPa) lower than that of the lab data. The minimum porosity point is also slightly shifted towards lower clay content values compared to the lab data. This indicates that the models are not able to provide accurate porosity estimations in the transition between the grain-supported and matrix-supported regime. One of the underlying assumptions of the models is that the sand lattice will

not be disturbed as the pore space is filled, and for the shale, that the sand grains will not disturb the shale packing. According to Marion et al. (1992) this is practically only valid for either very high or very low clay contents, which is likely to cause deviations when comparing the models with the lab data. Marion et al. (1992) have argued that this can be seen as a lower bound for porosity in a sand-clay mixture. This indicates that the porosity estimations in the transition between the grain-supported and matrix-supported regime will be underestimated, while the estimations provide more accurate results for clean sand and clean shale. This coincides with the findings when comparing the models to the lab data.

When plotting P-wave velocity as a function of porosity, it becomes evident that Dvorkin yields higher velocities than the modified BAM, as can be seen in Figure 5.2. Both models fail to capture the velocity-porosity trend in the transition between the grain-supported and matrix-supported regime, which is seen more clearly in Figure 5.3. Here it can be seen that the two models give a better estimate of the velocity-porosity trend at the end-points, while it starts to deviate when going into shaley sand and sandy shale. Again, it becomes evident that the models provide more accurate estimations for clean sand and clean shale than the transition between these two end points.

Figure 5.4 shows the P-wave velocity plotted against clay content for the two models, along with the results obtained from the lab experiment. Also here it becomes evident that the Dvorkin model yields higher velocities than the modified BAM. Both models overpredict the velocity, where the modified BAM and Dvorkin yield $3-12.6$ % and $7.5-24.2$ % higher velocities at the maximum velocity point than the lab data, respectively. The overestimation of velocities in the Dvorkin model is likely caused by the assumptions underlying granular models. As the grains are not spherical, and all surfaces are rough, the discrepancies from theoretical results may occur. The behaviour of rough contacts is a challenging problem (Misra and Huang, 2012), and is likely to contribute to the overestimation as roughness may cause a decrease of the bulk moduli of the outer part of the grain. The coordination number-based approach may also account for some errors in the estimation. Also, at higher stresses, some grain plastification may occur.

Furthermore, the peak velocity for both models is shifted towards lower clay content values relative to the lab data. This coincides with the shift towards lower clay contents for the minimum porosity points, which is assumed to be the underlying reason for the shift in the velocity-clay content plot. The peak velocity coincides with the minimum porosity point for both models.

6.2 Compared to Wells on the Norwegian Continental Shelf

When comparing the two models to well data, the general trend of the results is that the porosity estimation is better than the estimation of clay content. For all three wells, the porosity estimation is quite accurate, showing only small deviations. However, the porosity estimation shows deviations in the assumed overpressured zone, where it either underpredicts or overpredicts the porosity, as seen in Figures 5.12, 5.14, 5.17, 5.19, 5.22, and 5.24.

When overpressure is accounted for, the net stress in the models is lowered, or w for the modified BAM model, and this results in underprediction of the porosity, as seen in Figures 5.13, 5.15, 5.18, 5.20, 5.23, and 5.25. When σ' or w is lowered, the models are shifted downwards toward lower velocities. This causes the velocity plane to intersect the models at values corresponding to both lower porosity and clay contents. This happens because the velocity plane intersects the model in the shaley sand - sandy shale domain. In the assumed overpressured zones, the highest porosity in the models is found at clean shale. When moving towards lower clay contents, the porosity decreases, and this is likely the cause of the underpredictions of the porosity observed in these zones. The clay content estimations, however, become more accurate when accounting for overpressure. This may indicate that the models do not give an accurate description of the porosity-clay content relationship. As could be seen when compared to the lab data, the two models do not give an accurate description of this relationship, where the porosity is underpredicted for shaley sand and sandy shale, while the clay content is both over- and underpredicted in the same interval.

The sum of volumetric fractions of clay, sand, and porosity has to be equal to one at all times. Keeping this in mind, it should be assumed that an underprediction of porosity would cause an overprediction of clay content. This is, however, not the case. As can be seen in Figure 5.24, the porosity is slightly overpredicted in the overpressured zone, and in the same zone, the clay content is also overpredicted. As the highest possible modeled porosity in this zone is the start porosity of shale, high porosities will result in a lithology close to clean shale. If this is the case, the sand content will be low, causing the clay content to be high. This is likely to be the reason for some of the deviations observed in the wells.

This further indicates that the two models do not fully capture the trend of the mixture. The models conceptualize a complex problem in a simple way, and as could be

seen when compared to lab data, the models do not entirely capture the trend of the transition between grain-supported and matrix-supported regime, making it difficult to obtain accurate lithology estimations.

It is very important to note that the two models only account for sand and clay. The wells mostly consist of these two constituents (Statoil, 1993; Norsk Hydro A.S., 1982; Saga Petroleum A.S., 1985), but there are also other mineralogies present, such as carbonates, coal, etc. These other mineralogies are likely to cause deviations in the estimations, and most likely accounts for some of the discrepancies observed. Furthermore, it is assumed full water saturation when modeling, but there are hydrocarbon shows in all wells (Norsk Hydro A.S., 1982; Statoil, 1993; Saga Petroleum A.S., 1985). This will account for some of the discrepancies in the results. In addition, the under- and overprediction of the clay content may also be due to a wrongful estimation of V_{cl} from the GR-log.

It is also possible that some of the deviations are caused by the assumption of dispersed mixing of the two constituents. If the mixing is laminar, the porosity calculations made in the two models are not valid, and the estimated porosities will be significantly lower compared to a laminar mixing mode. In addition, it is worth noting that there could have been chosen a wrongful estimation of the sand- and shale porosities when modeling. This is especially likely for the smectite-rich intervals, which show anomalously high porosities.

When comparing the two models to the lab data, the modifed BAM gave the best results. Dvorkin tended to overpredict the velocities more than the modifed BAM. As the modified BAM introduces the anisotropy term, it is likely to assume that this model would be the better fit. However, when comparing to well data, this is not necessarily the case. When comparing the models to well 6608/10-3 the modified BAM gives the best results (see Figures 5.14 and 5.15), while Dvorkin gives the best results for both well 33/5-2 (see Figures 5.17 and 5.18) and 34/7-1 (see Figures 5.22 and 5.23). This may be caused by the simplicity of the explicit pressure term in the Dvorkin model. Well 6608/10-3 have been calibrated, making it easy to estimate w when using the modified BAM. However, for the two other wells, the calibration from well 6608/10-3 is used along with the velocity information to make assumptions of how w may vary with depth. It may seem as it is harder to make a good estimate of w, rather than inserting the net stress from the pressure trends plots.

For well 33/5-2 the modeled estimations start to deviate with increasing depth. At about 2500-3000 mbsf, the porosity estimations become overpredicted, as seen in Figures 5.22

and 5.24. In this area, chemical compaction is likely to occur (Walderhaug, 1996; Lander and Walderhaug, 1999). Chemical compaction causes smectite to transform to illite and chlorite, and cementation occurs. This will cause a decrease in the porosity and an increase in the velocity. As the two models do not account for chemical compaction (they are only valid for the mechanical compaction domain), they will not be applicable in this area. It can be seen that the models fail to follow the general clay trend in this area, which should be assumed due to the assumptions underlying the two models.

The strength of the models resides in the minimal information needed to perform estimations, as only P-wave velocity is used as an input parameter. Both models are able to give an overview of the general porosity and clay trends in the wells tested. As sand-clay mixtures are hard to model, the two models give an easy way of conceptualizing and modeling a complex problem, and they could provide useful information of the general trends observed. As for all models, the information obtained may be of greater value as more parameters are accounted for, but in this case it was chosen to maintain the simplicity of the models.

Chapter 7

Conclusion

Two models have been created and used to predict porosity and clay content solely based on P-wave velocity. The models explain the relationship between porosity, clay content, and compressional velocities, and were created by taking base in a binary system consisting of sand and clay subject to dispersed mixing.

Dvorkin's Textural Sorting takes base in the ratio between large (sand) and small (clay) grains, and the elastic moduli is calculated using Hertz-Mindlin and Hashin-Shtrikman bounds. The modified BAM is based on the Voigt and Reuss bounds, and takes anisotropy into account.

When tested on lab data, both models underpredict the porosity and overpredict the velocity in the transition between the grain-supported and the matrix-supported regime. The Dvorkin model yields a stiffer result than the modified BAM, and overpredicts the velocities with 7.5 - 24.2 % compared to the lab data.

Both models are able to predict the general porosity and clay trends when tested on well data, but show deviation in the estimation in the overpressured zones. When accounting for overpressure, the porosity estimation is underpredicted for both models, but the estimation of clay content becomes more accurate. The models fail to accurately describe the transition between the grain-supported and the matrix-supported regime.

The modified BAM shows better results than Dvorkin when compared to lab data, where Dvorkin gives a stiffer result, overprediciting the velocities more than what can be ob-

served for the modified BAM. However, when tested on well data, Dvorkin yields better results for two of the three wells tested. This is likely caused by the w introduced in the modified BAM, which seems to be more difficult to assign compared to the explicit pressure term used in the Dvorkin model. The modified BAM yields better results when tested on the calibrated well.

The two models fails to accurately describe the transition between the grain-supported regime and the matrix-supported regime, but offers a simple way to conceptualize a complex problem. The strength of the two models resides in the minimal need of P-wave velocity to perform estimations. The modified BAM yields better results when more information can be used to estimate w, whereas the Dvorkin model has its strength in the explicit pressure term used to make predictions. The minimal need of information needed allows the models and methodology to be used on numerous data sources, and they could possibly be used for both exploration and production purposes.

Chapter 8

Further Work

In the previous sections it has been shown how the modified BAM and Dvorkin's Textural Sorting can be used to predict porosity and clay trends based on compressional velocities.

As the models are only tested on lab data and well data, the next step would be to test the models on seismic data.

This work is also limited by only being applicable in the mechanical compaction domain. It would be interesting to further extend the models to account for chemical compaction.

Bibliography

Avseth, P., Mukerji, T., Mavko, G., and Dvorkin, J. (2010). Rock-physics diagnostics of depositional texture, diagenetic alterations, and reservoir heterogeneity in high-porosity siliciclastic sediments and rocks - a review of selected models and suggested work flows. *Geophysics*, 75(5):75A31–75A47.

Dvorkin, J. and Gutierrez, M. (2001a). Grain sorting, porosity, and elasticity. *Geophysics Department, Stanford University*.

Dvorkin, J. and Gutierrez, M. A. (2001b). Textural sorting effect on elastic velocities, part ii: elasticity of a bimodal grain mixture. *SEG Technical Program Expanded Abstracts*, pages 1764–1767.

Dvorkin, J. and Nur, A. (2002). Critical-porosity models. *AAPG Memoir*, 76:33–41.

Hashin, Z. and Shtrikman, S. (1963). A variational approach to the elastic behavior of multiphase materials. *Journal of Mechanics and Physics of Solids*, 11:127–140.

Lander, R. and Walderhaug, O. (1999). Predicting porosity through simulating sandstone compaction and quartz cementation.

Marcussen, , Thyberg, B. I., Peltonen, C., Jahren, J., Bjørlykke, K., and Faleide, J. (2009). Physical properties of cenozoic mudstones from the northern north sea: Impact of clay mineralogy on compaction trends. *AAPG Bulletin*, 93(1):127–150.

Marion, D. and Nur, A. (1991). Pore-filling material and its effect on velocity in rocks. *Geophysics*, 56(2):225–230.

Marion, D., Nur, A., Yin, H., and Han, D. (1992). Compressional velocity and porosity in sand-clay mixtures. *Geophysics*, 57(4):554–563.

Mavko, G., Mukerji, T., and Dvorkin, J. (2009). *The Rock Physics Handbook, Second Edition*. Cambridge University Press.

Mindlin, R. D. (1949). Compliance of elastic bodies in contact. *Journal of Applied Mechanics*, 16:259–268.

Misra, A. and Huang, S. (2012). Micromechanical stress-displacement model for rough interfaces: Effect of asperity contact orientation on closure and shear behavior. *International Journal of Solids and Structures*, 49:111–120.

Norsk Hydro A.S. (1982). Final Well Report Well 33/5-2. Last Accessed June 17 2017 from http://www.npd.no/engelsk/cwi/pbl/wellbore_documents/405_1_Completion_Report_and_Completion_log.pdf.

NPD. NPD Factpages. Last Accessed June 17 2017 from http://factpages.npd.no/ReportServer?/FactPages/PageView/wellbore_exploration&rs:Command=Render&rc:Toolbar=false&rc:Parameters=f&NpdId=1732&IpAddress=129.241.228.133&CultureCode=nb-no.

NPD. NPD Factpages. Last Accessed June 17 2017 from http://factpages.npd.no/ReportServer?/FactPages/PageView/wellbore_exploration&rs:Command=Render&rc:Toolbar=false&rc:Parameters=f&NpdId=111&IpAddress=129.241.228.133&CultureCode=nb-no.

NPD. NPD Factpages. Last Accessed June 17 2017 from http://factpages.npd.no/ReportServer?/FactPages/PageView/wellbore_exploration&rs:Command=Render&rc:Toolbar=false&rc:Parameters=f&NpdId=405&IpAddress=129.241.229.47&CultureCode=nb-no.

Nur, A., Mavko, G., Dvorkin, J., and Galmudi, D. (1998). Critical porosity: A key to relating physical properties to porosity in rocks. *The Leading Edge*, 17(3):357–362.

Peltonen, C., Marcussen, , Bjørlykke, K., and Jahren, J. (2008). Mineralogical control on mudstone compaction: a study of late cretaceous to early tertiary mudstones of the vøring and møre basins, norwegian sea. *Petroleum Geoscience*, 14:127–138.

Raymer, D., Hunt, E., and Gardner, J. (1980). An improved sonic transit time-to-porosity transform.

Saga Petroleum A.S. (1985). Final Well Report 34/7-1. Last Accessed June 17 2017 from http://www.npd.no/engelsk/cwi/pbl/wellbore_documents/111_01_34_7_1_Completion_Report_and_Log.pdf.

Statoil (1993). Completion Report Well 6608/10-3 PL 128. Last Accessed June 17 2017 from

http://www.npd.no/engelsk/cwi/pbl/wellbore_documents/1732_6608_10_3_COMPLETION_REPORT_AND_LOG.pdf.

Storvoll, V., Bjørlykke, K., and Mondol, N. (2005). Velocity-depth trends in mesozoic and cenozoic sediments from the norwegian shelf. *AAPG Bulletin*, 89(3):359–381.

Vernik, L. and Kachanov, M. (2010). Modeling elastic properties of siliciclastic rocks. *Geophysics*, 75(6):E171–E182.

Walderhaug, O. (1996). Kinetic modeling of quartz cementation and porosity loss in deeply buried sandstone reservoirs.

Wang, Z. (2001). Fundamentals of seismic rock physics. *Geophysics*, 66(2):398–412.

Wood, A. (1941). A textbook of sound. *Macmillan Publ. Co.*

Wyllie, M., Gregory, A., and Gardner, L. (1956). Elastic wave velocities in heterogeneous and porous media. *Geophysics*, 21:41–70.

Appendix A

Additional Information

A.1 Additional Well Information

In this section, additional well information and values used in the modeling are found.

A.1.1 Well 6608/10-3

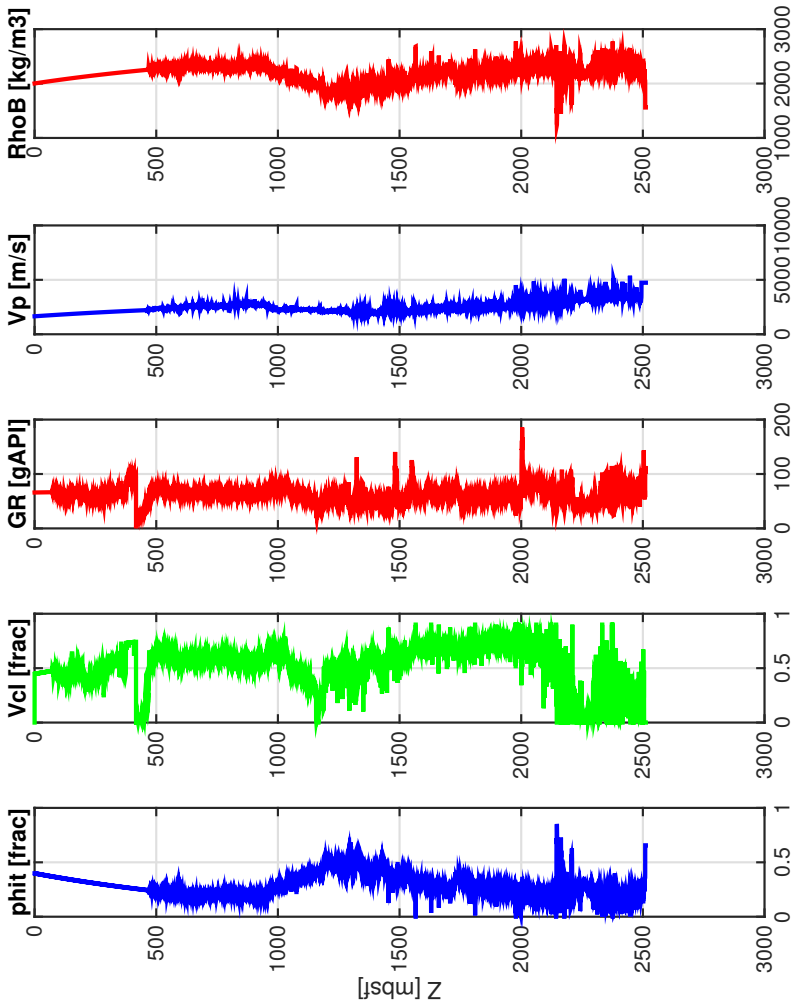

Figure A.1: The figure shows the logs obtained from well 6608/10-3.

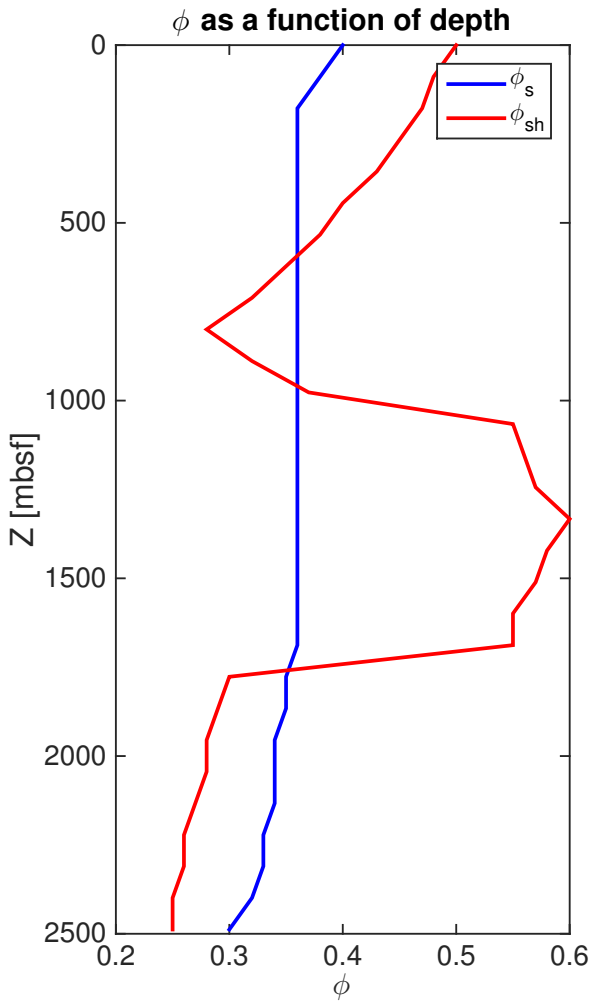

Figure A.2: The figure shows the values of ϕ_s and ϕ_{sh} that are used in the modeling.

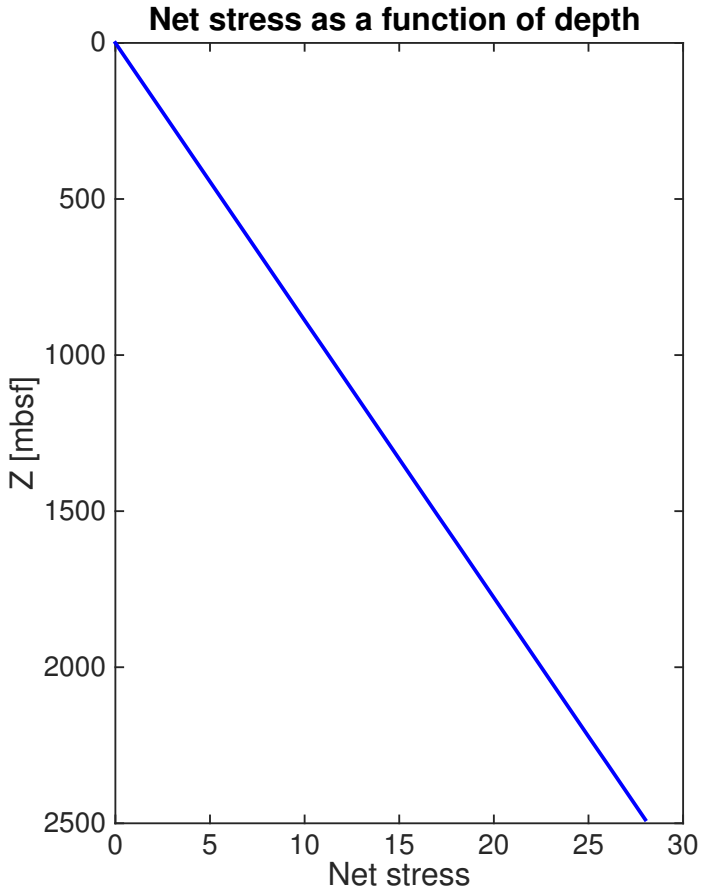

Figure A.3: The figure shows the net stress as a function of depth used in the modeling.

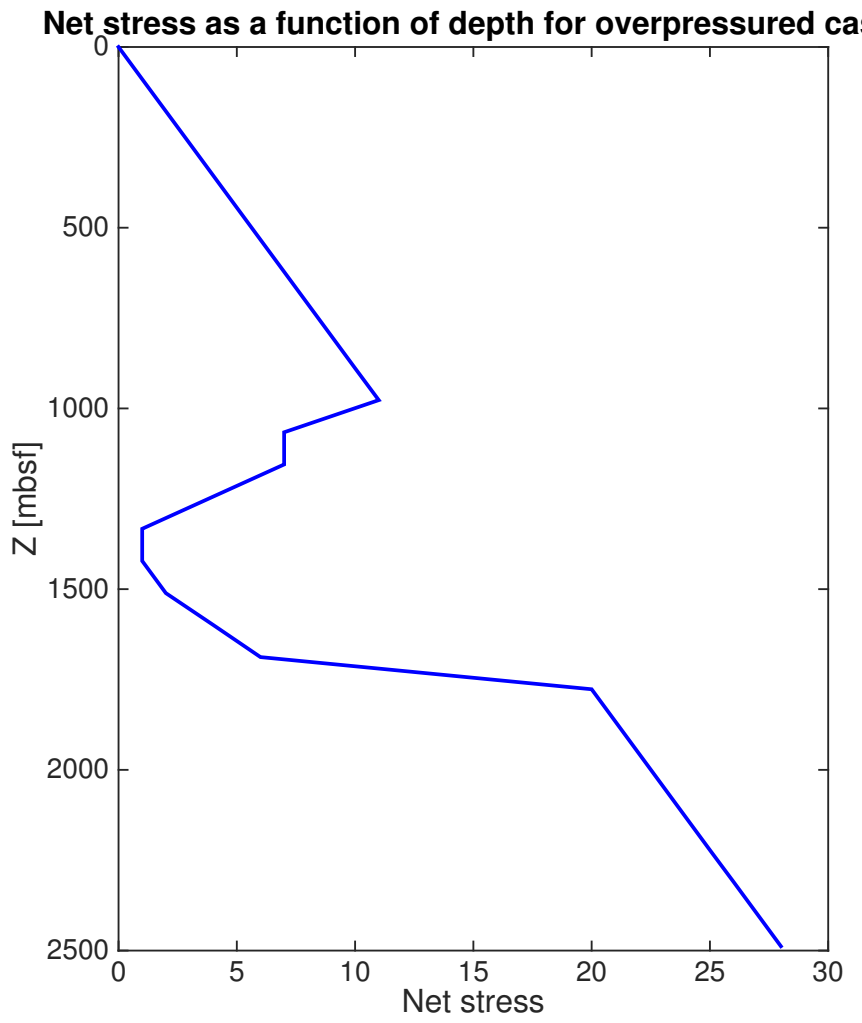

Figure A.4: The figure shows the net stress as a function of depth used in the modeling when assuming overpressure.

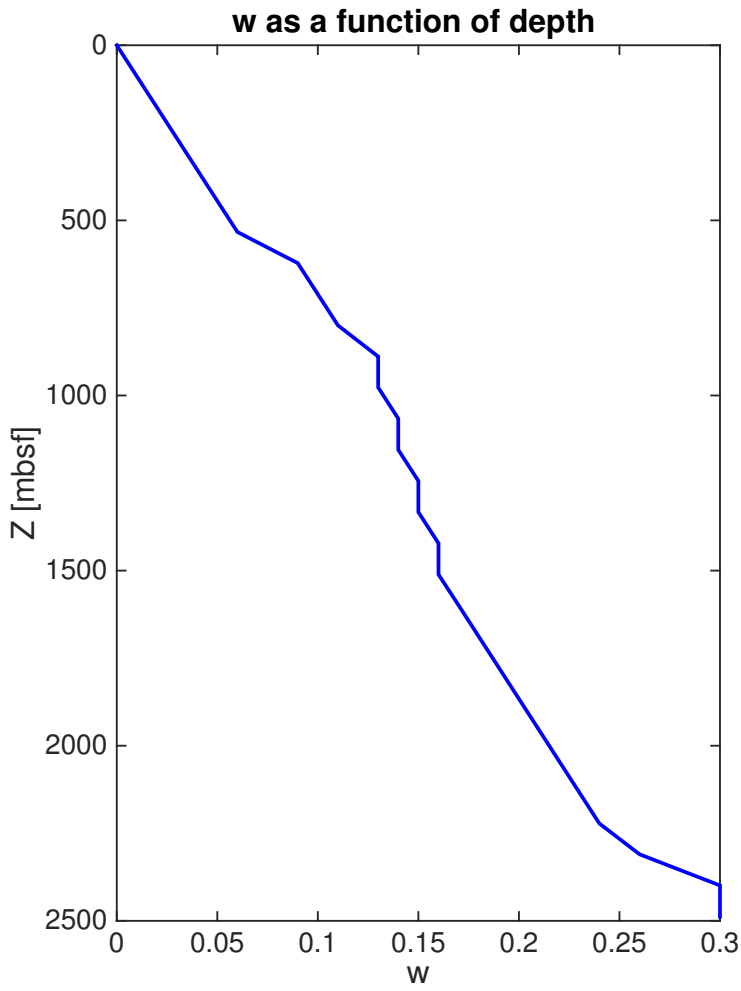

Figure A.5: The figure shows w as a function of depth used in the modeling.

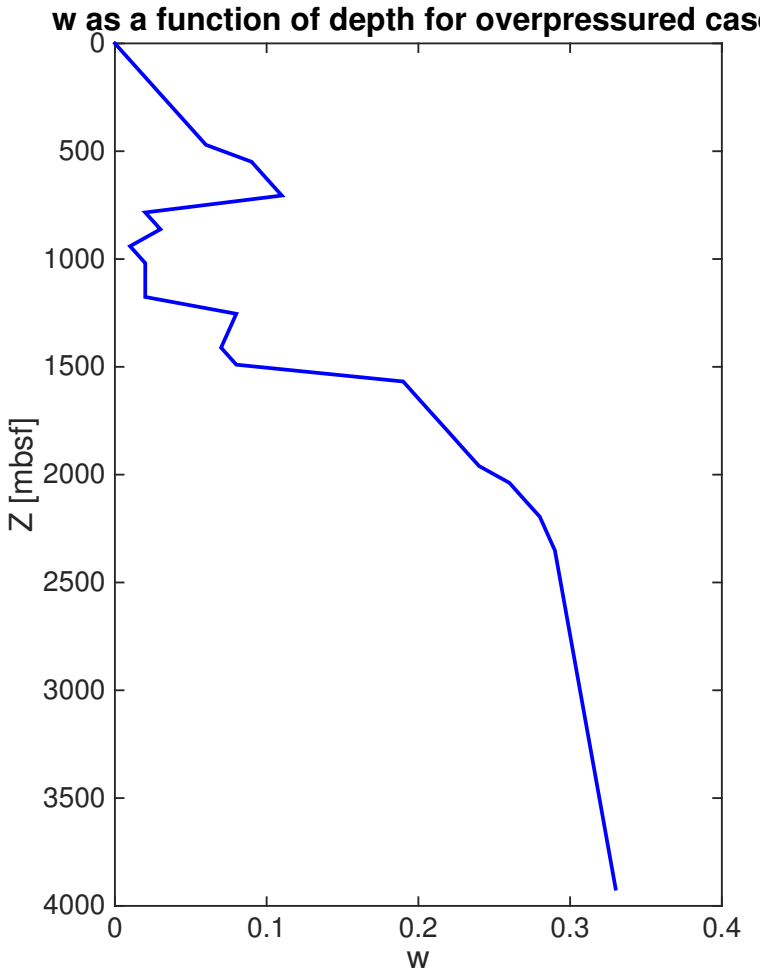

Figure A.6: The figure shows w as a function of depth used in the modeling when assuming overpressure.

A.1.2 Well 34/7-1

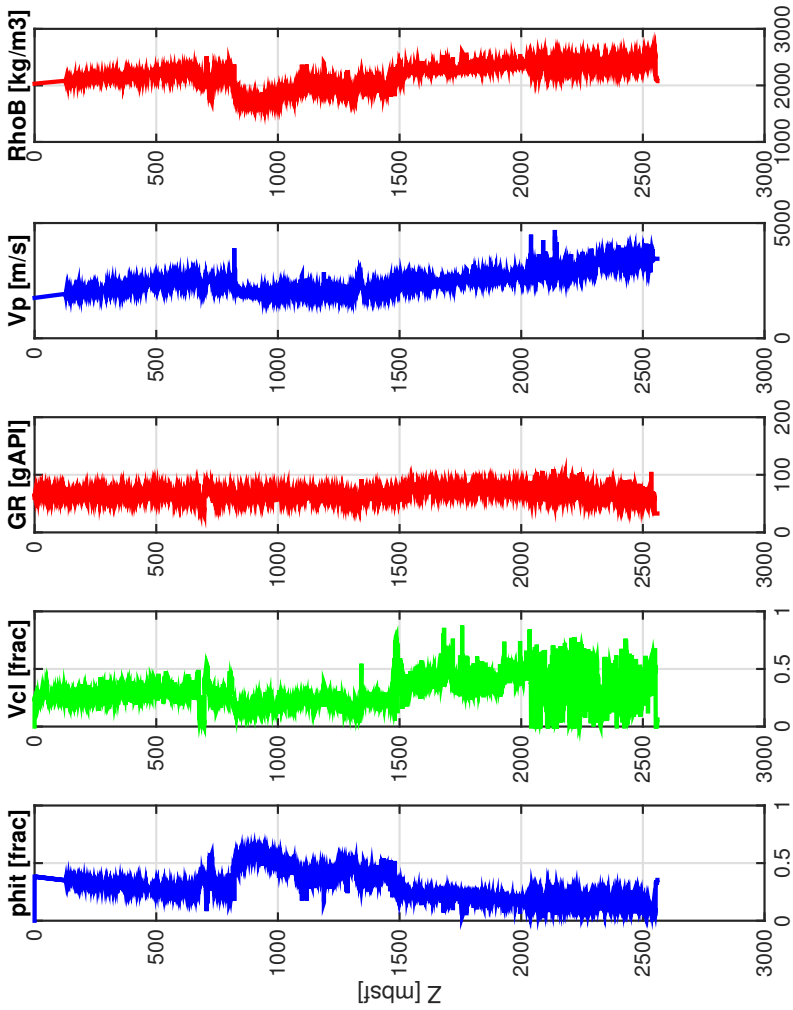

Figure A.7: The figure shows the logs obtained from well 6608/10-3.

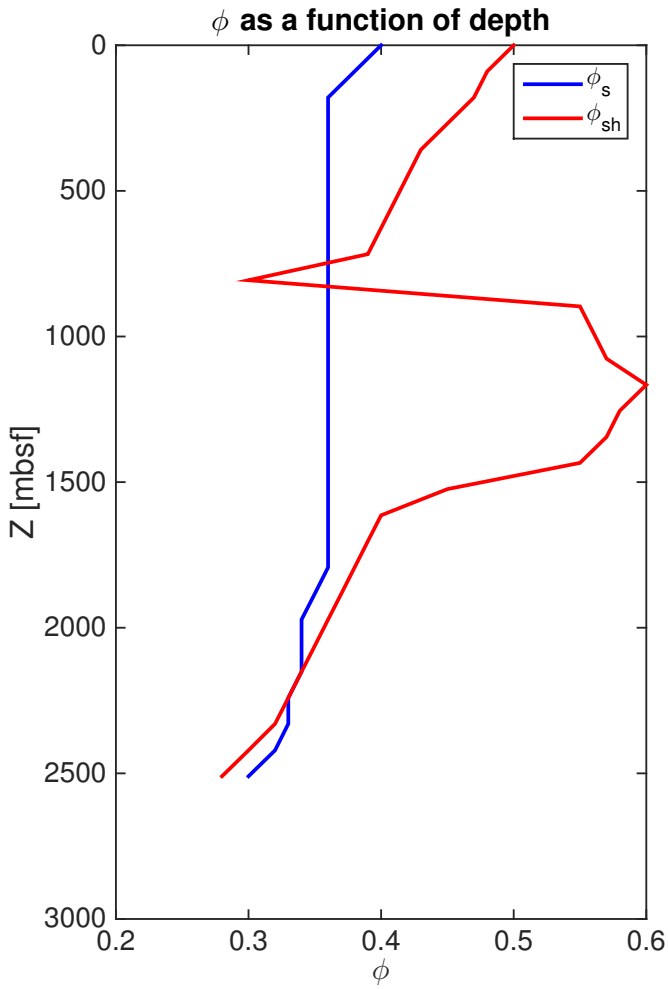

Figure A.8: The figure shows the values of ϕ_s and ϕ_{sh} that are used in the modeling.

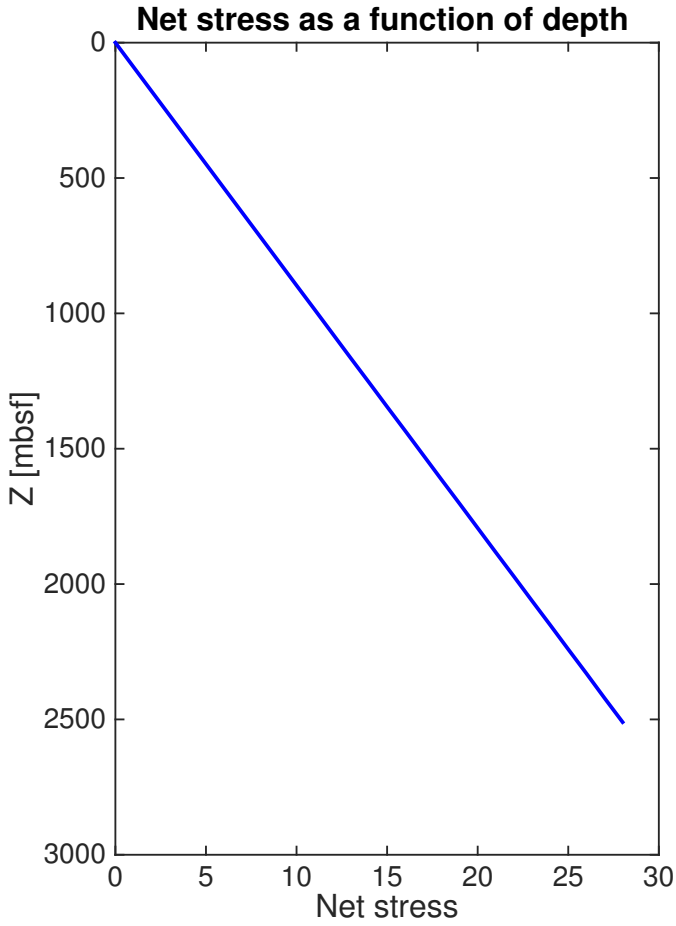

Figure A.9: The figure shows the net stress as a function of depth used in the modeling.

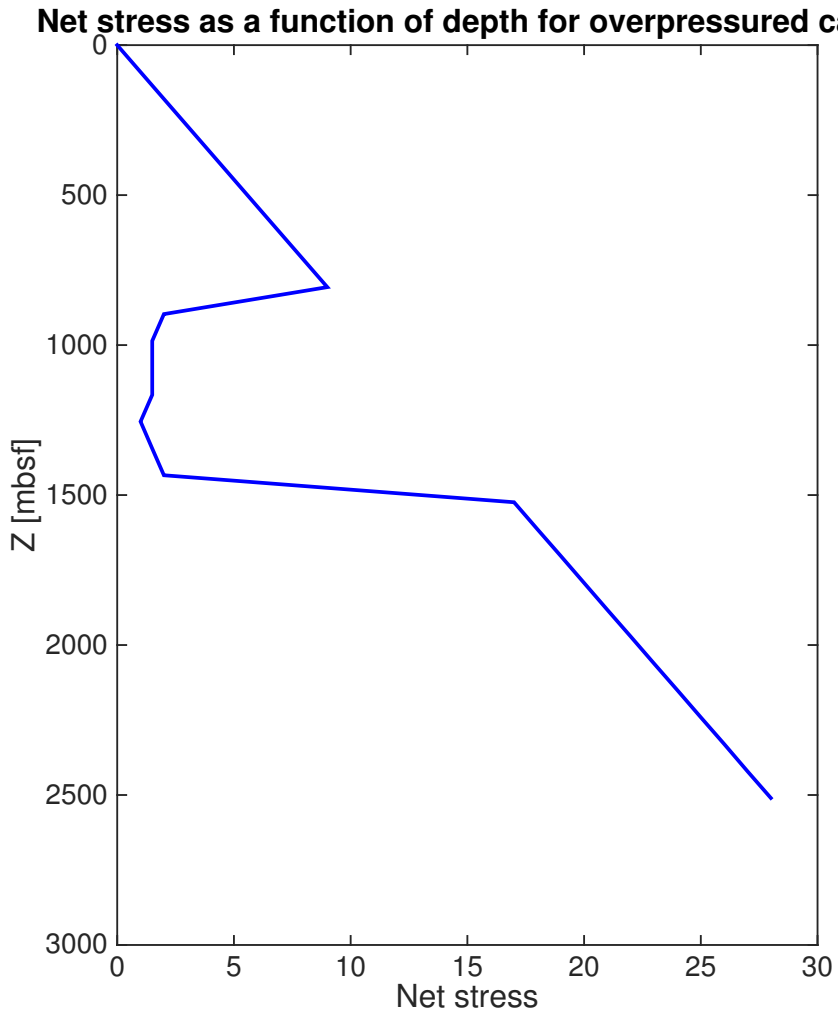

Figure A.10: The figure shows the net stress as a function of depth used in the modeling when assuming overpressure.

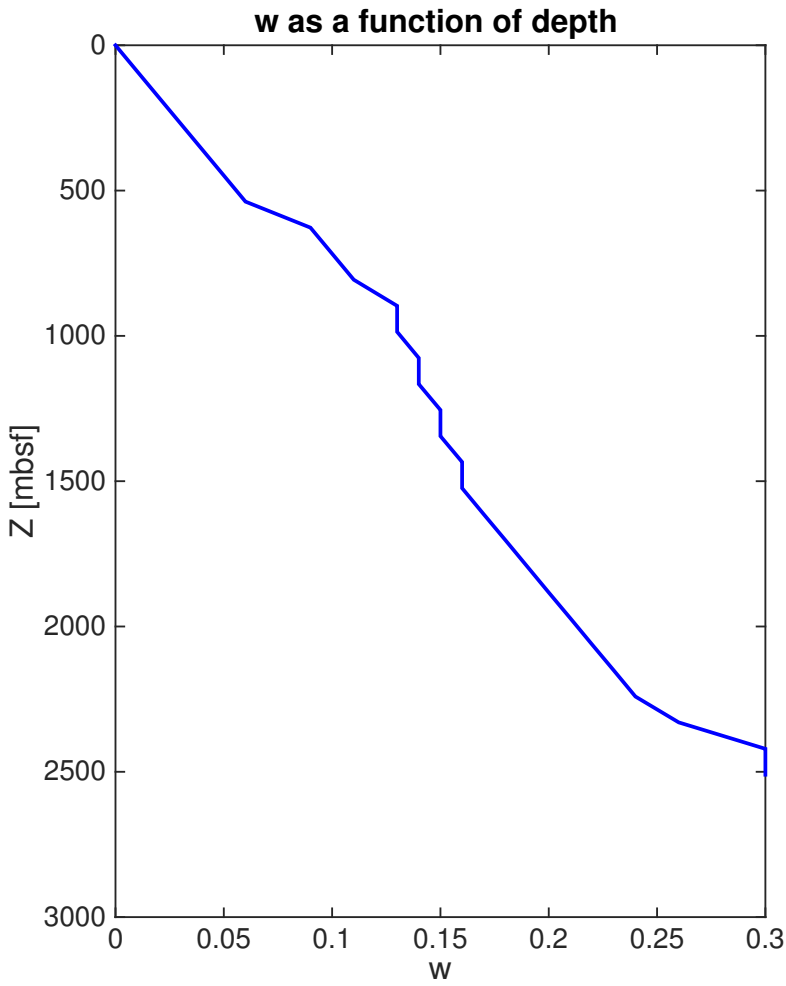

Figure A.11: The figure shows w as a function of depth used in the modeling.

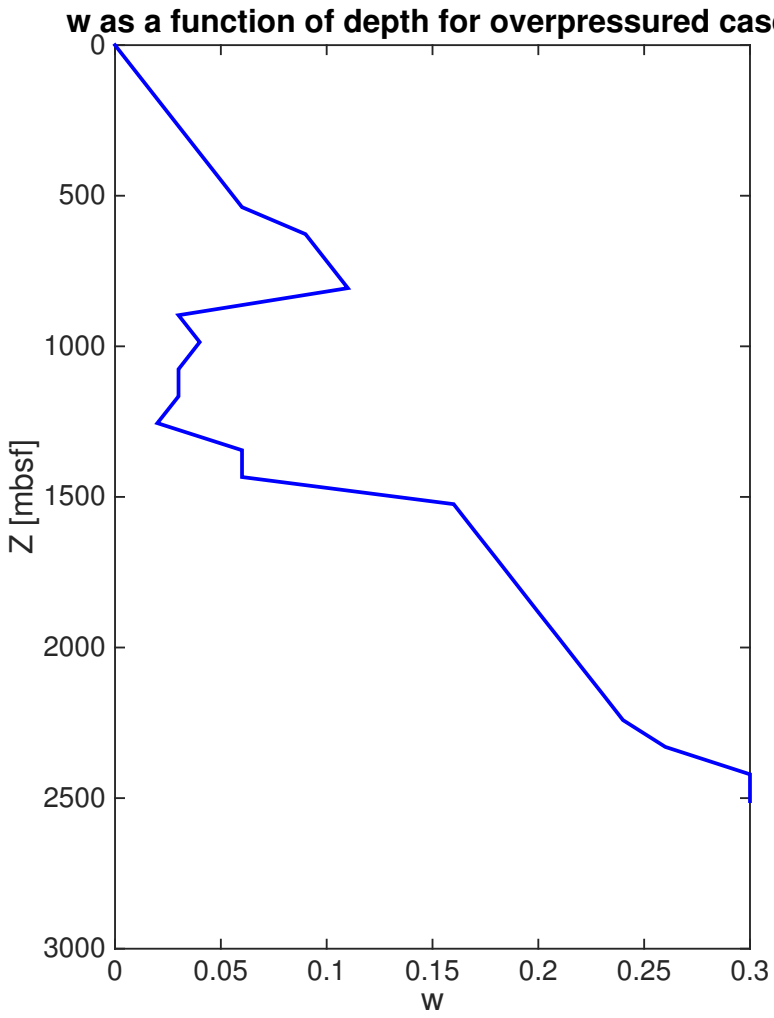

Figure A.12: The figure shows w as a function of depth used in the modeling when assuming overpressure.

A.1.3 Well 33/5-2

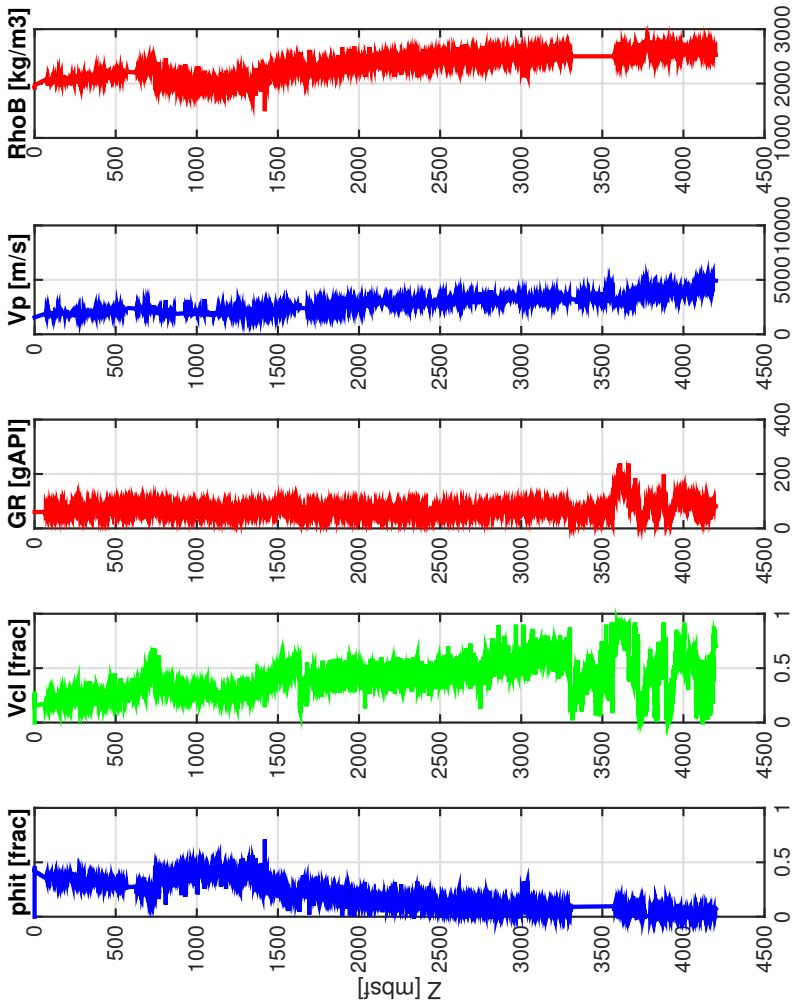

Figure A.13: The figure shows the logs obtained from well 6608/10-3.

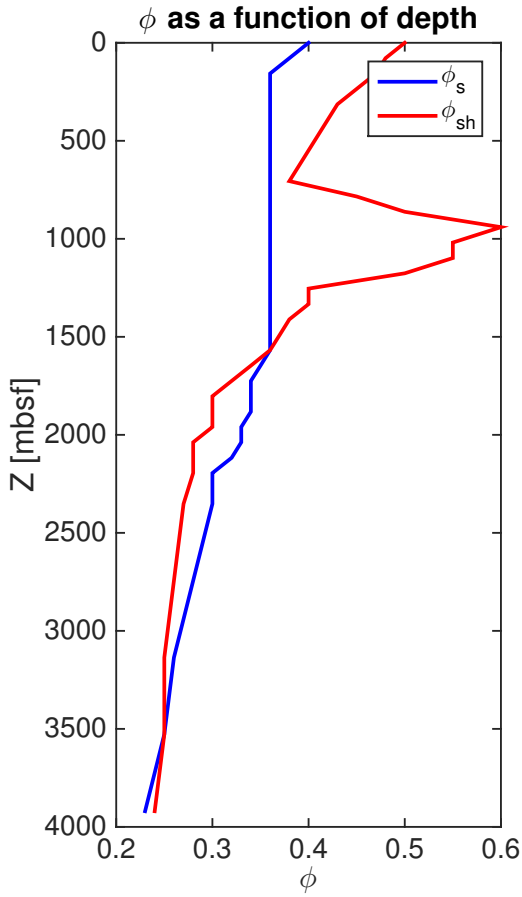

Figure A.14: The figure shows the values of ϕ_s and ϕ_{sh} that are used in the modeling.

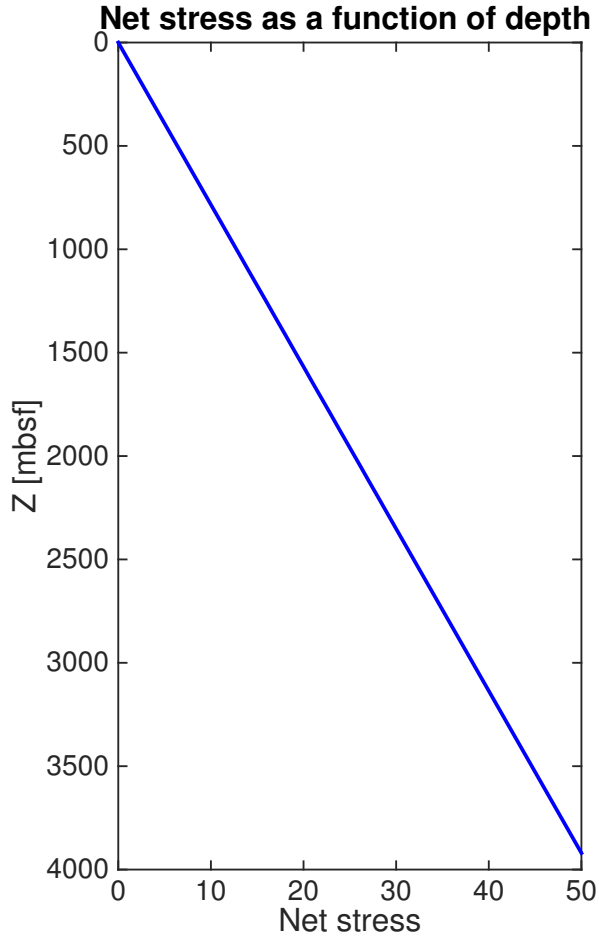

Figure A.15: The figure shows the net stress as a function of depth used in the modeling.

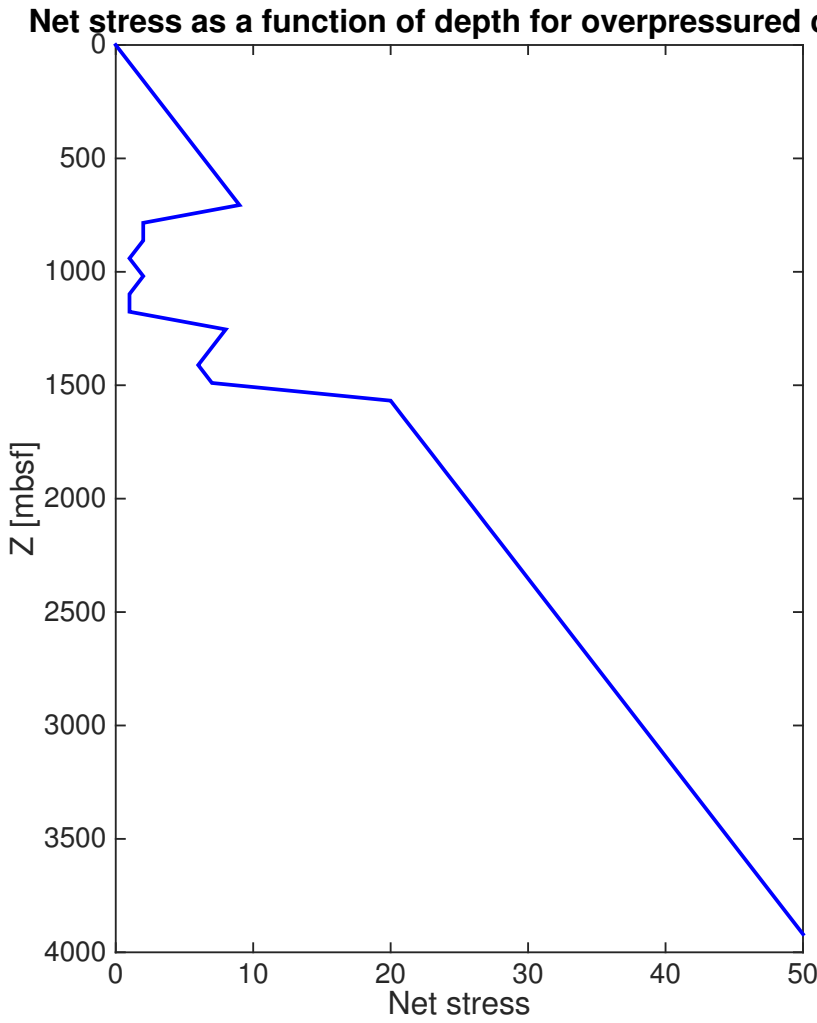

Figure A.16: The figure shows the net stress as a function of depth used in the modeling when assuming overpressure.

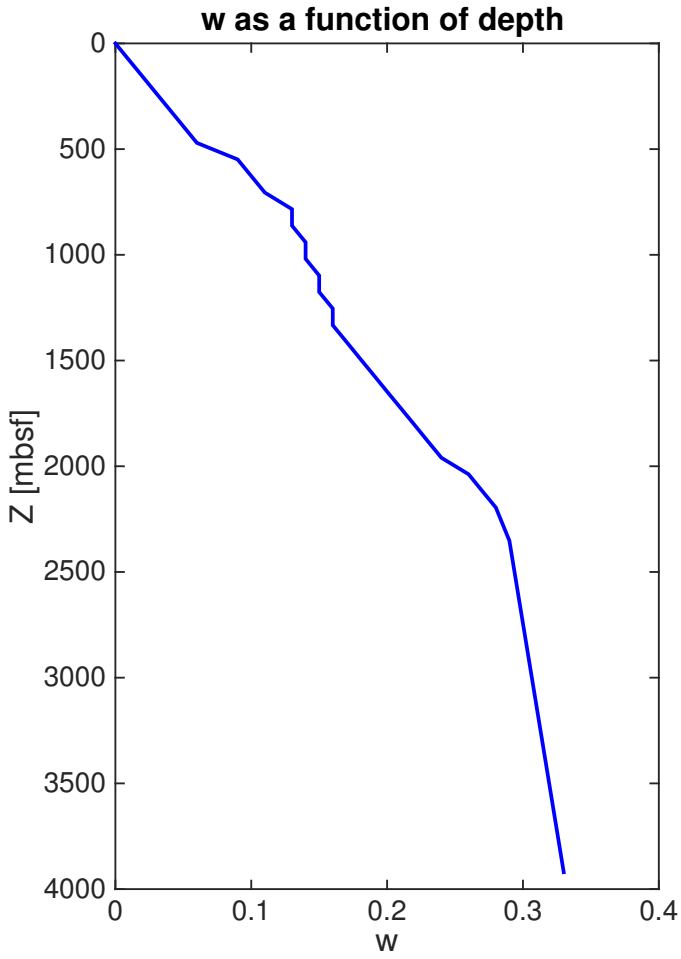

Figure A.17: The figure shows w as a function of depth used in the modeling.

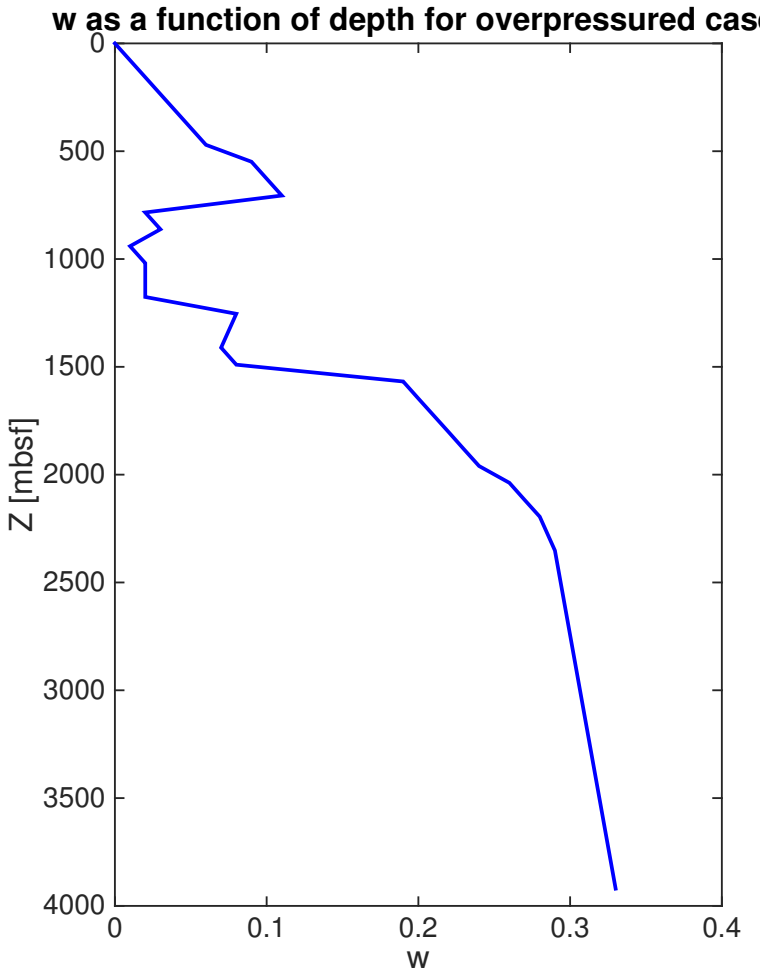

Figure A.18: The figure shows w as a function of depth used in the modeling when assuming overpressure.